Palaeogeography, Palaeoclimatology, Palaeoecology 475 (2017) 140–153

Contents lists available at ScienceDirect

Palaeogeography, Palaeoclimatology, Palaeoecology

journal homepage: www.elsevier.com/locate/palaeo

Inter-annual climate variability in Europe during the Oligocene icehouse

Walliser E.O. [a,*], Lohmann G. [b,c], Niezgodzki I. [b,d], Schöne B.R. [a]

[a] Institute of Geosciences, University of Mainz, Johann-Joachim-Becher-Weg 21, 55128 Mainz, Germany
[b] Alfred Wegener Institute, Helmholtz Centre for Polar and Marine Research, Am Alten Hafen 26, 27568 Bremerhaven, Germany
[c] Institute of Environmental Physics and Marum, University of Bremen, Bremen, Germany
[d] ING PAN - Institute of Geological Sciences Polish Academy of Sciences, Research Center in Kraków, Senacka 1, 31-002 Kraków, Poland

ARTICLE INFO

Article history:
Received 13 January 2017
Received in revised form 16 March 2017
Accepted 20 March 2017
Available online 21 March 2017

Keywords:
Sclerochronology
Climate models
North Atlantic Oscillation
Quasi-decadal
Carbon isotopes

ABSTRACT

New sclerochronological data suggest that a variability comparable to the North Atlantic Oscillation (NAO) was already present during the middle Oligocene, about 20 Myr earlier than formerly assumed. Annual increment width data of long-lived marine bivalves of Oligocene (30–25 Ma) strata from Central Europe revealed a distinct quasi-decadal climate variability modulated on 2–12 (mainly 3–7) year cycles. As in many other modern bivalves, these periodic changes in shell growth were most likely related to changes in primary productivity, which in turn, were coupled to atmospheric circulation patterns. Stable carbon isotope values of the shells ($\delta^{13}C_{shell}$) further corroborated the link between shell growth and food availability. Sub-decal oscillations in the 3–7 year band in other annually resolved fossil archives were often interpreted as El Niño-Southern Oscillation (ENSO) cycles. This possibility is discussed in the present study. However, combined shell-derived proxy and numerical climate model data lend support to the interpretation of a NAO-like variability. According to numerical climate models, winter sea-level pressure (wSLP) and precipitation rate (wPR) across Central Europe during the Oligocene exhibited a pattern similar to the modern NAO. The simulated NAO index for the Oligocene shows periodicities coherent with those revealed by the proxy data (2.5–6 years), yet, on shorter wavelengths than the modern NAO (biennial and 6–10 year cycles). Likely, the different paleogeography and elevated atmospheric CO_2 concentrations not only influenced the sea-level pressure pattern, but also the temporal variability of the NAO precursor. The present study represents the first attempt to characterize the inter-annual climate variability in Central Europe during the Oligocene and sets the basis for future studies on the early phase of the Cenozoic icehouse climate state.

1. Introduction

The Eocene/Oligocene boundary marks the shift of global climate from the early Paleogene Greenhouse to the modern icehouse state (Miller et al., 1991; Zachos et al., 2008). The resulting pervasive climate deterioration particularly affected the Northern Hemisphere, leading to the largest marine and terrestrial faunal turnover of the Cenozoic era in Europe (Prothero, 1994; Prothero et al., 2003), also known as the *Grande Coupure* (Stehlin, 1909). Previous studies suggested that climatic changes across the North Atlantic sector and Central Europe significantly contributed to this event (e.g., Ivany et al., 2000; Eldrett et al., 2009; Mosbrugger et al., 2005; Kocsis et al., 2014). For example, according to palynological data, mean annual and winter temperatures dropped by ca. 3 to 10 °C (Mosbrugger et al., 2005; Erdei et al., 2012) between the late Eocene and the early Oligocene (Rupelian). A similar trend was reconstructed from the oxygen isotope composition of terrestrial rodent teeth phosphate (Héran et al., 2010). Likely, climate cooling in Central Europe was related to a change of the source of atmospheric masses across the continent. Numerical model simulation and proxy data suggest that until the Eocene, central European atmospheric masses originated from the Tethys and the Pacific Ocean (e.g., Bice et al., 2000; Kocsis et al., 2014). As indicated by varved sediments, atmospheric circulation was controlled by the ENSO during this time interval (Mingram, 1998; Lenz et al., 2010). However, $\delta^{18}O$ data from terrestrial mammals from Europe show a trend toward negative values from the Eocene to the Oligocene (Héran et al., 2010; Kocsis et al., 2014) suggesting a shift of the source of the atmospheric moisture toward the North Atlantic during the Late Paleogene. This time interval coincides with the major uplift phase of the Alps (Kuhlemann, 2007), which likely acted as an atmospheric barrier to the Tethyan realm and the Pacific climate (Kocsis et al., 2014). This configuration resembles the modern situation with the westerlies being the major trajectory of Central European atmospheric masses (Hurrell and Deser, 2009). Today, the interannual climate variability of Europe is largely influenced by sea-level pressure (SLP) dynamics across the North Atlantic, i.e., the North Atlantic Oscillation. As indicated by annually resolved $\delta^{18}O$ data from corals (Brachert et al., 2006; Mertz-Kraus et al., 2009), speleothems (e.g., Scholz et al., 2012) and laminated lacustrine sediments (Muñoz et al., 2002; Kloosterboer-Van Hoeve et al., 2006), the NAO existed already

* Corresponding author.
E-mail address: walliser@uni-mainz.de (E.O. Walliser).

http://dx.doi.org/10.1016/j.palaeo.2017.03.020
0031-0182/

during the Neogene. The oldest currently available evidence for such a NAO precursor comes from $\delta^{18}O$ records of late Miocene corals for the Mediterranean (Brachert et al., 2006; Mertz-Kraus et al., 2009). However, Miocene periodic cycles in the thicknesses of halovarves from Italy have also been interpreted as reflecting ENSO rhythms (Galeotti et al., 2010). Due to the lack of specific studies, it is still unknown whether the Oligocene inter-annual climate variability was influenced by ENSO or possibly by a precursor of the NAO. A promising approach to test this hypothesis is to study annual shell growth patterns of long-lived bivalves from shallow marine deposits of the Oligocene and compare their inherent frequencies to numerical paleoclimate models that are able to simulate short-term dynamics.

Shells of bivalve mollusks form by periodic accretion of calcium carbonate and serve as unique physical and chemical archives of past environmental conditions (e.g., Ivany, 2012; Schöne, 2013). Typically, the skeletons do not grow continuously through the year, but biomineralization slows down or even halts once a year (e.g., Clark, 1974; Witbaard et al., 1994) resulting in the formation of distinct annual growth lines (e.g., Checa, 2000). These annual lines divide the shell growth pattern into equal time slices known as annual growth increments. Many studies have shown that changes in the width of the growth increments of bivalves are linked to temperature, food availability and food quality (e.g., Ambrose et al., 2006; Witbaard et al., 1997), and in turn, can be used to reconstruct these environmental variables. Long-lived species are particularly suitable for increment width-based climate reconstructions (Marchitto et al., 2000; Strom et al., 2004; Schöne et al., 2005; Black et al., 2008; Butler et al., 2013). Standardized annual shell growth data (= standardized growth indices, SGI) of long-lived *Glycymeris glycymeris* and *Arctica islandica* provided information about the variability of the NAO (Schöne et al., 2003; Holland et al., 2014; Reynolds et al., 2017) and ENSO (e.g., Ivany et al., 2011) in the more recent past and in deeper time.

Here, we present annual shell growth data of three long-lived bivalve species, *G. planicostalis*, *G. obovata* and *A. islandica* collected from Oligocene strata of four different localities in Central Europe located between Germany and Belgium. In addition, we performed fully coupled numerical climate simulations to evaluate the atmospheric circulation dynamics and their spatial extent during that time. Proxy data and simulated NAO indices were then compared by means of spectral analysis. Furthermore, shell stable oxygen ($\delta^{18}O_{shell}$) and carbon isotope ($\delta^{13}C_{shell}$) data of one *Glycymeris* sp. specimen were used to evaluate possible links between shell growth and environmental variables (temperature and food availability).

2. Geological setting, shell material and methods

2.1. Geological setting and shell material

Due to the combined effect of eustatic rise and tectonic subsidence related to the Alpine collision, Central Europe repeatedly experienced regional marine transgressions from the paleo North Sea during the Oligocene. This led to the formation of several small epicontinental basins and widespread deposition of fossil-rich sand deposits along the paleocoastlines formed by Paleozoic continental blocks (Berger et al., 2005a, 2005b). The strongest marine transgression occurred during the Rupelian between the sea-level highstands Ru2/Ru3 (~32 Ma) and Ru3/Ru4 (~29.5 Ma) of Haq et al. (1988). However, marine transgressions of minor intensity persisted during the Chattian (late Oligocene) and well into the Miocene (Berger et al., 2005a, 2005b). The studied strata formed during such transgressive intervals over much of the Oligocene epoch (ca. 31–25 Ma), and comprise the Rupelian deposits of the Bilzen Formation (Southern North Sea Basin, Belgium), the Alzey Formation and Stadecken Formation (Mainz Basin, Upper Rhine Graben, Germany), as well as the Chattian Kassel Formation, (Kassel Basin, Hesse Depression, Germany) (Fig. 1A and B).

The stratigraphic context and the origin of the investigated material are summarized in Table 1. Shells from Belgium (*Glycymeris obovata*, n = 2) were provided by the Naturalis Biodiversity Center of the National Museum of Natural History of The Netherlands and originated from the Mommen sand pit near Vliermaal (50°50′16.8″N, 5°25′40.8″E). The studied deposits belong to the Berg Sand Member, the lowest part of the Bilzen Formation. The Bilzen Formation represent the nearshore

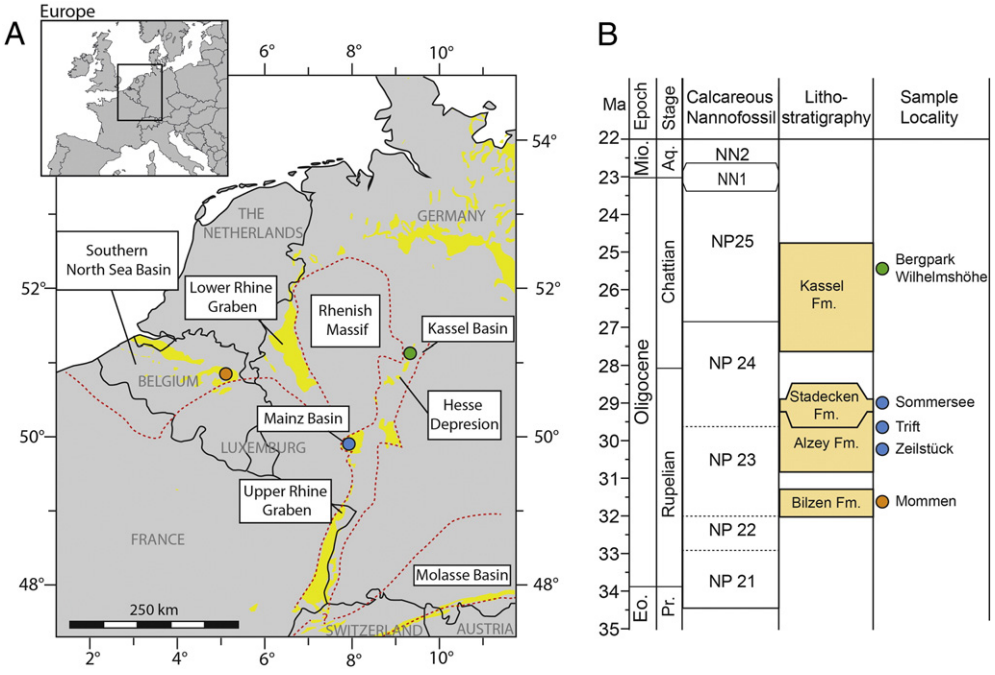

Fig. 1. Geographical and stratigraphic position of the studied areas in Germany and Belgium. (A) Geographic position of the studied localities (Southern North Sea Basin = orange circle; Mainz Basin = blue circle; Kassel basin = green circle). The contour of the paleocoastline is shown by the red dotted line. Whereas, the yellow areas show the distribution of Oligocene shallow marine deposits in Germany and Belgium. (B) Chronostratigraphic position of the studied lithostratigraphic units and localities.

Table 1
Studied fossil taxa used for calculation of standardized growth indices (SGI_{shell}).

Taxon	Sampled locality	Coordinates	Stratigraphy	# of shells
Glycymeris obovata	Southern North Sea Basin (Belgium)	50°50′16.8″N, 5°25′40.8″E	Bilzen Fm. (Rupelian)	2
	Kassel Basin (Germany)	51°19′11.04″N, 9°24′36.04″E	Kassel Fm. (Chattian)	6
Glycymeris planicostalis	Mainz Basin (Germany)	49°48′46.4″N, W8°8′32.0″E	Stadecken Fm. (Rupelian)	3
	Mainz Basin (Germany)	49°44′24.2″N, 8°04′20.4″E 49°44′49.4″N, 8°3′28.9″E	Alzey Fm. (Rupelian)	5
Arctica islandica	Mainz Basin (Germany)	49°44′49.4″N, 8°3′28.9″E	Alzey Fm. (Rupelian)	1

equivalent of the lower and middle part of the Boom Formation (Van Simaeys and Vandenberghe, 2006), which, in turn, encompasses the lower part of the nanoplankton zone NP23 (Vandenberghe et al., 2004) (Fig. 1B).

The Rupelian and Chattian material from Germany belonged to the paleontological collection of the University of Mainz. The Rupelian shells (*G. planicostalis*, n = 9; *Arctica islandica*, n = 1) were collected from the outcrops 'Trift' and 'Zeilstück' near Weinheim (49°44′24.2″N, 8°04′20.4″E and 49°44′49.4″N, 8°3′28.9″E, respectively: Alzey Formation) as well as the locality 'Sommersee' near Spiesheim (49°48′46.4″N, W8°8′32.0″E: Stadecken Formation), Rhineland-Palatinate. The Alzey Formation and the Stadecken Formation represent nearshore marine deposits of the Mainz Basin and are slightly younger than the Bilzen Formation. The deposits of the Alzey Formation comprise the upper part of the nanoplankton zone NP23 and the lower part of the NP24 (Martini, 1982; Grimm et al., 2011). The overlaying deposits of the Stadecken Formation fall within the middle part of the nanoplankton zone NP24 (Grimm et al., 2011) (Fig. 1B).

The Chattian shells (*G. obovata*, n = 6) were collected from temporary outcrops excavated in the Bergpark Wilhelmshöhe, Kassel, Germany (51°19′11.04″N, 9°24′36.04″E). Deposits belong to the Kassel Formation and encompass the upper part of the nanoplankton zone NP24 and the lower part of NP25 (Roth, 1970; Martini and Müller, 1971; Ritzkowski et al., 2011) (Fig. 1B). $^{87}Sr/^{86}Sr$ chemostratigraphy (McArthur et al., 2001; regression curves LOWESS version 5, 26 March, 2013) performed on a well-preserved *G. obovata* shell from these deposits yielded an age of 25.5 ± 0.5 Ma (Walliser et al., 2016) (Fig. 1B).

2.2. Shell preparation

Firstly, the shell material was mounted on Plexiglas cubes using Gluetec Multipower plastic welder and wrapped in a protective layer of WIKO metal epoxy resin to avoid breakage during sectioning. Sectioning was performed along the axis of maximum growth (Fig. 2A) with a low-speed precision saw (Buehler Isomet 1000; 225 rpm) equipped with a 0.4 mm-thick diamond-coated blade. From each shell, two 3 mm-thick slabs were cut and successively attached to glass slides with the mirroring side facing up. The slabs were then repeatedly ground on glass plates using 320, 800, and 1200 grit SiC powder and finally polished with a 1 μm Al_2O_3 powder. Between each step, slabs were ultrasonically rinsed with water. In order to facilitate the recognition of internal growth structures, one slab of each sample was immersed in Mutvei's solution for 40 min at 37–40 °C (Schöne et al., 2005) (Fig. 2B). Thereafter, samples were carefully rinsed with deionized water and air-dried.

2.3. $\delta^{13}C_{shell}$ and $\delta^{18}O_{shell}$ analysis

Diagenetic overprint could potentially alter the pristine $\delta^{18}O_{shell}$ and $\delta^{13}C_{shell}$ signature of fossil material. The preservation of the studied bivalve shell was tested in a previous study (Walliser et al., 2015) with a plethora of different analytical techniques (immersion in Feigl's solution, cathodoluminescence, scanning electron microscopy). Carbonate powder samples (50–120 μg) for stable isotope analysis were collected from the outer shell layer of the valve of specimen MB-Wht-2, MB-Wht-4 and MB-Wht-7of Walliser et al. (2015; Mainz Basin). In order to gain information about the $\delta^{13}C_{shell}$ during later ontogenetic years, specimen MB-Wht-4 was newly sampled. In this case, sampling resolution ranged between 7 and 1 data point per annual growth increment and covers age 2 to 40 of life of the organism. Sampling was performed by milling under a stereomicroscope using a Rexim Minimo dental drill equipped with a 1 mm thick cylindrical diamond coated bit (Gebr. Brasseler GmbH & Co. KG, model number 835104010).

Stable oxygen and carbon analysis was performed using a Thermo Finnigan MAT 253 continuous flow isotope ratio mass spectrometer coupled to a GasBench II at the Institute of Geosciences, University of Mainz. Carbonate powders were dissolved in Helium flushed borosilicate exetainers with water-free phosphoric acid at 72 °C. Isotope data were then calibrated against an NBS-19 calibrated Carrara marble ($\delta^{13}C = +2.01‰$; $\delta^{18}O = -1.91‰$) distributed by IVA-Analysentechnik e.K. (Germany). For both the $\delta^{13}C$ and $\delta^{18}O$ values, the internal precision (1σ) and the accuracy (external reproducibility) were better than 0.05‰, respectively. Results of the analysis are expressed in typical δ-notation and given in ‰ (per mil) with respect to the VPDB (Vienna Pee Dee belemnite) standard.

The $\delta^{18}O_{shell}$ data of the studied shell were already published by Walliser et al. (2015) and were used to reconstruct the seasonal water temperature in the shallow water of the Rupelian Mainz Basin. Temperatures ($T_{\delta 18O}$) were calculated using the paleothermometry equation of Grossman and Ku (1986) with scale correction of Dettman et al. (1999) assuming a $\delta^{18}O$ signature of the water of −0.9‰ (Walliser et al., 2015). These data were used in the present study for the calculation of the seasonal shell growth rates.

2.4. Reconstruction of seasonal growth rates

In order to reconstruct seasonal shell growth rates, incremental $T_{\delta 18O}$ values were aligned to modeled seasonal seawater temperature (T_{mod}) curves computed with a monthly resolution (12 data points)

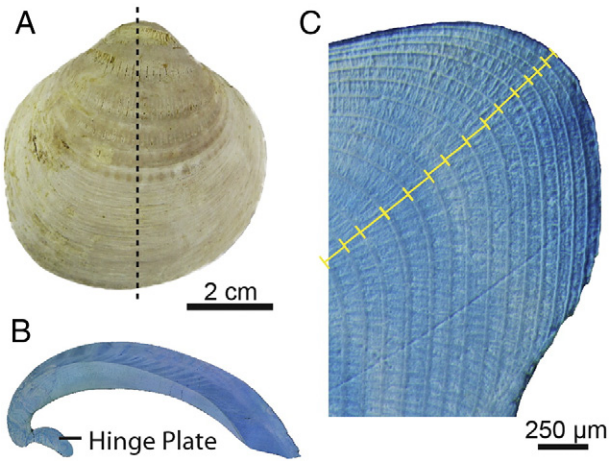

Fig. 2. Preparation of the studied shells. (A) An example of *Glycymeris planicostalis* shell from the Mainz Basin. Dotted line indicates cutting axis. (B) Image of a *Glycymeris planicostalis* shell slab stained with Mutvei's solution, and (C) magnification of the hinge plate where growth increment width were measured (yellow bars).

using a sinusoidal equation. Since the studied *Glycymeris* spp. bivalves grew their shells over winter and summer (Walliser et al., 2015, 2016) it was possible to extrapolate the full seasonal water temperature amplitude to which the animals were exposed during growth. To account for the interannual variability of the seasonal seawater temperature amplitudes, each growth increment was treated separately. Accordingly, the minimum and maximum $T_{\delta 18O}$ values from each growth year were used to constrain the amplitude of the T_{mod} curve used for data alignment. To facilitate the arrangement of the $T_{\delta 18O}$ data on the T_{mod} curve, we computed 3rd to 6th order polynomial functions to the $T_{\delta 18O}$ data. After the temporal alignment, seasonal shell growth rates were calculated as percentage of the respective year.

2.5. Reconstruction of relative annual growth increment widths

The stained samples were photographed with a Canon EOS 600D digital camera mounted on a Wild Heerbrugg M8 binocular microscope at 12× magnification. Growth increment widths were measured in the hinge plate (Fig. 2C) using the image processing software Panopea (©Peinl and Schöne) and used to construct age-detrended and standardized annual shell growth data (= standardized growth indices, SGI) following the procedure of Schöne (2003). The ontogenetic trends of the shell accretion rates were estimated for each shell with a highly adaptive 4-year spline. Growth indices (GI) were calculated by dividing each measured growth value (R_t) by the predicted (P_t) value for the corresponding year.

$$GI = \frac{G_t}{P_t} \quad (1)$$

The resulting GI chronologies were then standardized as follows:

$$SGI = \frac{GI - \mu}{\sigma} \quad (2)$$

where μ and σ are the average and standard deviation of all GI values, respectively.

2.6. Numerical climate simulations

Numerical climate simulations were performed with the Earth System Model COSMOS for pre-industrial (Stepanek and Lohmann, 2012; Wei et al., 2012) and Oligocene conditions. The model configuration includes the atmosphere component ECHAM5 at T31 resolution (~3.75°) with 19 vertical layers (Roeckner et al., 2006). The ocean component MPI-OM, including the dynamics of sea ice formulated using viscous-plastic rheology, has an average horizontal resolution of 3° × 1.8° with 40 uneven vertical layers (Marsland et al., 2003). The model was validated against observational data and the last millennium (Jungclaus et al., 2006; and references therein). It was furthermore compared to proxy data for the Holocene (Lohmann et al., 2013), Eemian (Pfeiffer and Lohmann, 2016; Felis et al., 2015), glacial millennial-scale variability (Zhang et al., 2014; Abelmann et al., 2015; Werner et al., 2016), and warm climates in the Miocene (Knorr et al., 2011; Knorr and Lohmann, 2014) and Pliocene (Dowsett et al., 2013; Salzmann et al., 2013). The model's ability to simulate different climates and its sensitivity to forcing has further been evaluated in several model intercomparisons (Varma et al., 2012; Lunt et al., 2013; Haywood et al., 2013; Bakker et al., 2014; Weber et al., 2014; Kageyama et al., 2012).

In our Oligocene simulations, we employed the paleogeography compiled by GETECH company that created paleogeographies representing periods of the Earth history with different paleoshorelines (for further details see: Lunt et al., 2013). Based on this paleogeography, we have prepared the boundary conditions necessary to run the model (cf. Stepanek and Lohmann, 2012). Boundary conditions included a global vegetation distribution, the set-up of the hydrological discharge model (Hagemann and Dümenil, 1998) and orography related parameters for the gravity wave drag parametrization (Lott and Miller, 1997). In accordance with previous proxy and model based estimations (Henderiks and Pagani, 2008; Walliser et al., 2016), Oligocene atmospheric carbon dioxide levels were set at 2 × PAL (560 ppm). This simulation is referred to as 'O-560' in the following. To investigate the effect of atmospheric radiative forcing on the winter sea-level pressure (wSLP) dynamics of the North Atlantic, an additional Oligocene simulation (O-280) was run at 1 × PAL level (280 ppm). The coupled atmosphere-ocean configuration was integrated for 3500 years in order to achieve climate steady state and avoid the artifacts on the deep ocean structures related to the model setup. Then, the last 100 years were taken for the analysis.

To extract the common signal of the model SLP data, an Empirical Orthogonal Function (EOF) analysis (von Storch and Zwiers, 2001) was applied to the model output. The aim of the EOF analysis technique is to find a new set of variables that captures most of the variance of the data through a linear combination of the original variables. Accordingly, the NAO is defined as the leading EOF (PC1) of the SLP across the North Atlantic sector (20°N-90°N, 90°W-70°E) (e.g., Hurrell and Deser, 2009). This method is alternative to the classical NAO index definition (the pressure anomaly differences between the Gibraltar and Iceland; e.g., Hurrell, 1995), however, it allows the calculation of all studied time slices regardless of their different land-ocean distribution. Accordingly, the 100-year long PC1 time-series were used to define the NAO-index in each simulation.

2.7. Spectral analysis

In order to reveal inherent shell growth dynamics in the studied fossils and to characterize the internal mode of variability of the simulated Oligocene atmospheric circulation patterns, the SGI_{shell} chronologies and NAO indices were analyzed by means of continuous wavelet transformation (CWT). CWT analysis was performed using the Matlab script of Torrence and Compo (1998; freely available at: http://paos.colorado.edu/research/wavelets/). Analysis was performed using Morlet wavelet (wavenumber = 6), whereas data were padded to zero. To evaluate the 5% significance level (i.e., the 95% confidence interval of the CWT powers) an univariate red-noise autoregressive lag-1 model was applied as a background spectrum. Therefore, powers above this significance interval can reasonably be considered free of randomly generated artifacts.

In order to explore possible teleconnection pathways between the tropical Pacific and the Central European climate during the Oligocene, we performed a coherency test between the CWT of the $NAO_{O\text{-}560}$ and ENSO $_{O\text{-}560}$ indices. For the test, we employed the Matlab script of Grinsted et al. (2004), using a Monte Carlo simulated univariate red-noise autoregressive lag-1 model for the identification of the 5% significant level. The ENSO index was computed using the 100-year long PC1 time-series of winter sea surface temperatures in the Central Pacific (30°N-30°S, 120°E-60°W).

3. Results

3.1. Bivalve $\delta^{13}C_{shell}$ data and seasonal growth rates

The $\delta^{18}O_{shell}$ and the $\delta^{13}C_{shell}$ high-resolution data cover 37 annual growth increments, spanning from age three to twenty-two of the bivalves of the Mainz (Fig. 3). The $\delta^{13}C_{shell}$ values fluctuate between −0.52 and +2.69‰ and clearly show an ontogenetic trend toward slightly positive values during the early ontogeny, followed by a trend toward more negative values in the later years (Fig. 3A). Annual minima, maxima and averaged $\delta^{13}C_{shell}$ data show positive correlation to the growth increment widths ($R^2 = 0.33$ and $p < 0.01$; Fig. 3B). The low resolution $\delta^{13}C_{shell}$ data chronology of specimen MB-Wht-4 compares very well with the high resolution data from the same specimen (Fig. 4A). Hence, the higher time averaging of the data seems not to compromise the quality of the

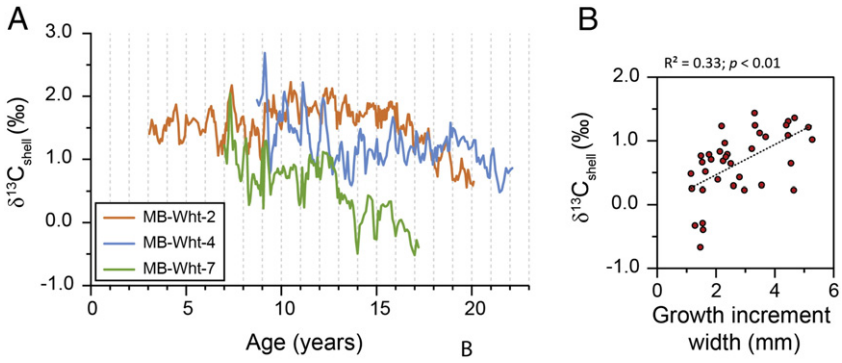

Fig. 3. Stable carbon isotope and growth increment width data from the studied glycymerids shells. (A) Stable carbon isotope data of *Glycymeris planicostalis* from the Rupelian deposits of the Mainz Basin (MB-Wht-2 = orange line; MB-Wht-4 = blue line; MB-Wht-7 = green line; respective $\delta^{18}O_{shell}$ values were published in Walliser et al. 2015). Vertical bars represent the position of the growth lines. (B) The bivariate linear model between annually averaged $\delta^{13}C_{shell}$ values and annual growth increment widths of the three bivalve shells of (A) show a positive correlation ($R^2 = 0.33$; $p < 0.01$).

chronology. The length of this chronology (39 years) allows to discern between early and a later ontogenetic phase in the $\delta^{13}C_{shell}$ data. The early phase (the first 20 years) is characterized by an average $\delta^{13}C_{shell}$ value of $+01.54 \pm 0.22‰$ ($\pm 1\sigma$) and show a positive correlation ($R^2 = 0.26$; $p < 0.03$) to the age-detrended growth increment width data (Fig. 4B). This phase is followed by four years (21–24) of strongly decreasing $\delta^{13}C_{shell}$ values, which then stabilize, around a more negative average value of $-0.01 \pm 0.28‰$ ($\pm 1\sigma$). From ontogenetic year 25 on, $\delta^{13}C_{shell}$ values show a negative correlation with age-detrended growth increment width data ($R^2 = 0.43$; $p < 0.01$) (Fig.4B). Reconstructed seasonal growth rates suggest that about 45% of the annual growth increment of the *glycymerids* was produced during winter and spring (Fig. 5).

3.2. Numerical climate simulations

The employed numerical climate models allow to extract seasonally resolved data from each simulated scenario (Pre-industrial: PI; Oligocene at $pCO_2 = 560$: O-560; Oligocene at $pCO_2 = 280$: O-280). In the following are reported data for winter seal level pressure (wSLP), precipitation rates (PR), and sea surface temperatures (wST). Climate models revealed the expected NAO-like patterns in the correlation maps between wSLP and local wPR (positive correlation over Greenland, negative correlation across Europe; Fig. 6A) as well as wSLP and winter surface temperatures (negative correlation over Iceland, positive correlation across Europe; wST; Fig. 6B) in the preindustrial simulation.

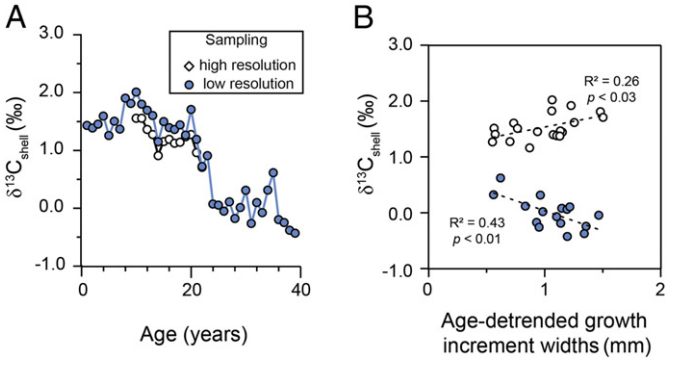

Fig. 4. Comparison between the high and low resolution $\delta^{13}C_{shell}$ chronology of specimen MB-Wht-4 and their correlation to age-detrended growth increment data. (A) The low-resolution time-series covers the first 39 years of specimen MB-Wht-4. For the overlapping growth years, the annual values of the low resolution series (blue dots) show a very good agreement with the high-resolution annually average $\delta^{13}C_{shell}$ data (white dots) derived from Fig. 3. (B) Annually averaged $\delta^{13}C_{shell}$ values of the first 20 ontogenetic years of specimen MB-Wht-4 correlate positively ($R^2 = 0.26$; $p < 0.03$) with the age-detrended shell growth data (white dots). However, an opposite trend (negative correlation; $R^2 = 0.43$; $p < 0.01$) is observed from age 25 onward (blue dots).

The O-560 simulation display similar results (Fig. 6C and D). However, the wSLP vs. wPR correlation patterns are more widespread (Fig. 6C), whereas wSLP vs. wST correlation patterns are geographically more restricted with the negative pattern mainly located over Southwest Greenland (Fig. 6D). A similar configuration is visible in the O-280 correlation maps, however, with geographical extensions matching those of the preindustrial simulation (Fig. 6E and F).

In the preindustrial simulation, the leading EOF analysis of the wSLP (PC1 = 45%) over the North Atlantic sector reveals the typical NAO configuration (NAO_{PI}) characterized by a positive and a negative pattern located north of Iberia and on eastern Greenland, respectively (Fig. 7A). A similar configuration is visible in the leading EOF analysis (PC1 = 34%) performed on the wSLP data of the O-560 simulation ($NAO_{O\text{-}560}$), yet its spatial distribution differs from the NAO_{PI} (Fig. 7B). The positive pattern is located at more northern latitudes (45°–55°N) than in the preindustrial control (40°–50°N), whereas the negative pattern is shifted by about 40° to the west. In the O-280 simulation, the leading EOF analysis of the wSLP data ($NAO_{O\text{-}280}$) exhibits two distinct negative patterns at high latitudes across Greenland and Eurasia, whereas the positive center of action appears less pronounced and flattened if compared to the other two simulations (Fig. 7C).

3.3. Spectral analysis

The SGI_{shell} chronologies are between 42 and 155 years long, and their CWT spectra display non-stationary significant signals, i.e., period length and intensity varied through time, between 2.1 and 11.7 year bands (Figs. 8 and 9). Significant powers at frequencies corresponding

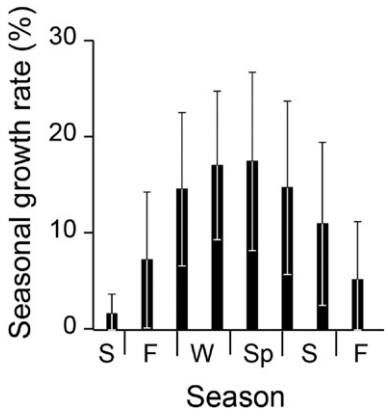

Fig. 5. Average seasonal shell growth rates reconstructed from the studied *Glycymeris planicostalis* shells. Average ($\pm 1\sigma$) seasonal growth rates were calculated using highly-resolved $\delta^{18}O_{shell}$ data from Walliser et al. (2015) and computed over a total of 40 individual growth increments. W = winter, Sp = spring, Su = summer, F = fall.

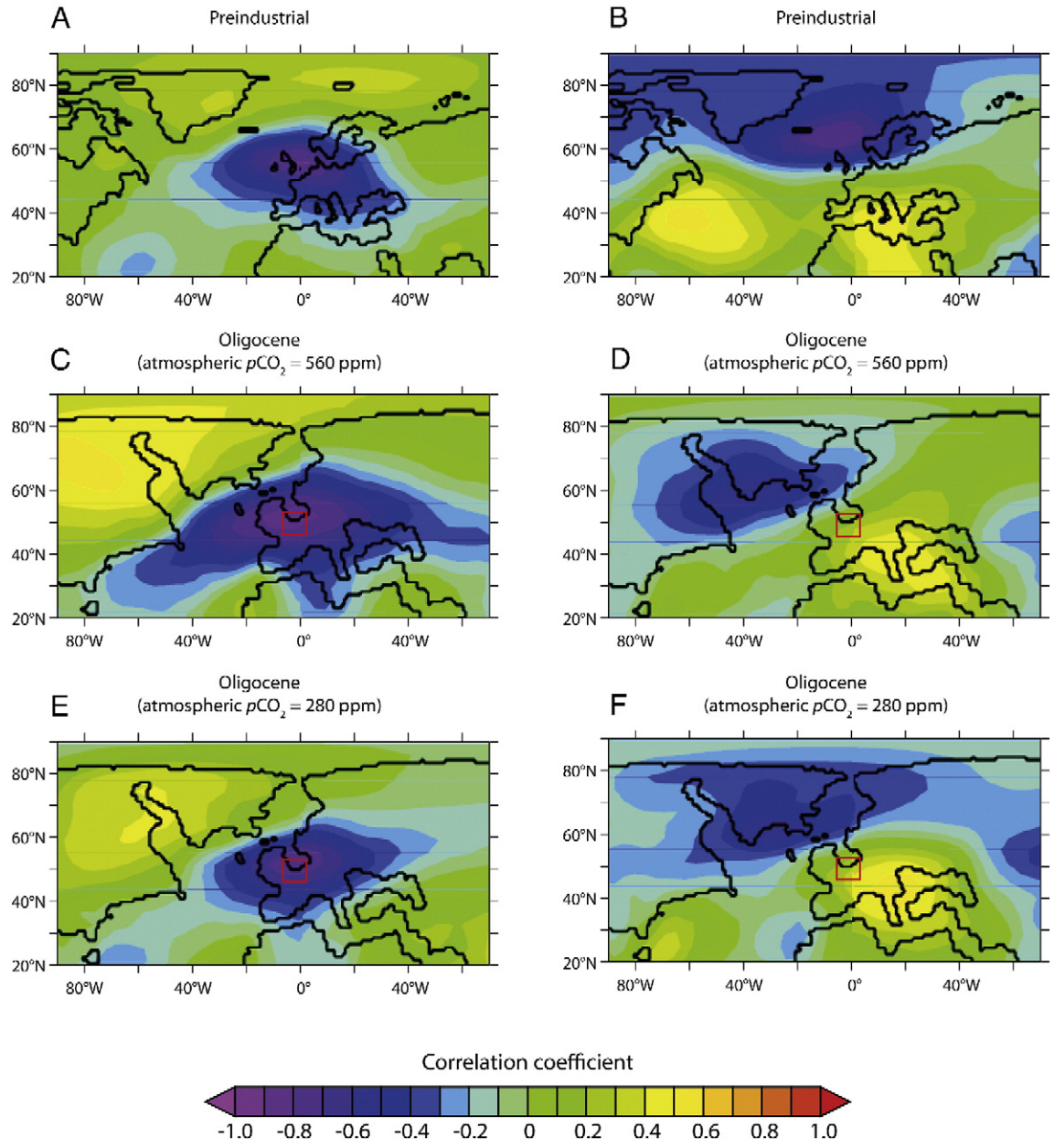

Fig. 6. Correlation maps between winter sea-level pressure and local precipitation rates (A, C and D) as well as winter sea-level pressure and local surface temperatures (B, D and F). Preindustrial (A and B) and both Oligocene O-560 (C and D) and O-280 (E and F) correlation maps show a pattern suggestive of interannual precipitation rates and surface temperatures variability in the North Atlantic sector was controlled by sea-level pressure. Red square shows the geographical position of the studied area.

to periods of 3–7 years occur in all CWT spectra (e.g., Figs. 8 and 9). Similar high-frequency periods occur in the simulated NAO indices, i.e., 3–5 years (NAO_{PI}), 2.5–5 years ($NAO_{O\text{-}560}$) and 2–6 years ($NAO_{O\text{-}280}$) (Fig. 10). Additionally, significant signals at lower frequencies are detected in the $NAO_{O\text{-}560}$ (8–16 years) and $NAO_{O\text{-}280}$ (9–12 years) index chronologies, but not in the NAO_{PI} index chronology (Fig. 9). The high powers around the 9 to 12 year bands visible in the CWT spectra of the NAO_{PI} index chronology partially fall outside the cone of influence; therefore, they are likely an artifact related to edge effects (Fig. 10A).

The coherency test between the CWT of the $NAO_{O\text{-}560}$ and $ENSO_{O\text{-}560}$ indices reveals patterns of significant correlations at sub-decadal and quasi-decadal timescales (Fig. 11A). However, the most pronounced pattern lay partially outside the cone of influence, and possibly, are the result of edge effects. At sub-decadal timescales, significantly coherent pattern are revealed in the 2–4 year band, however, with phase arrows pointing in opposite directions (Fig. 11B).

4. Discussion

The present study is the first to report on inter-annual climate variability of Central Europe during the Oligocene. Reconstructed shell growth rates combined with $\delta^{13}C_{shell}$ data suggest that the rates of shell formation of Oligocene glycymerids were coupled to variations of food availability (primary production). However, the results show that the incorporation of the environmental carbon into the shell was strongly influenced by physiological processes related to the ontogeny. Reconstructed seasonal growth rates display that a significant portion of the annual growth increments (ca. 45%) was formed during the colder season. This is the part of the year during which inter-annual changes in atmospheric conditions are more evident across in Central Europe. Shell growth (SGi_{shell}) data contain inherent frequencies within 2–12 year band (mainly within the 3–7 year band) which resemble the typical non-stationary behavior of atmospheric circulation patterns.

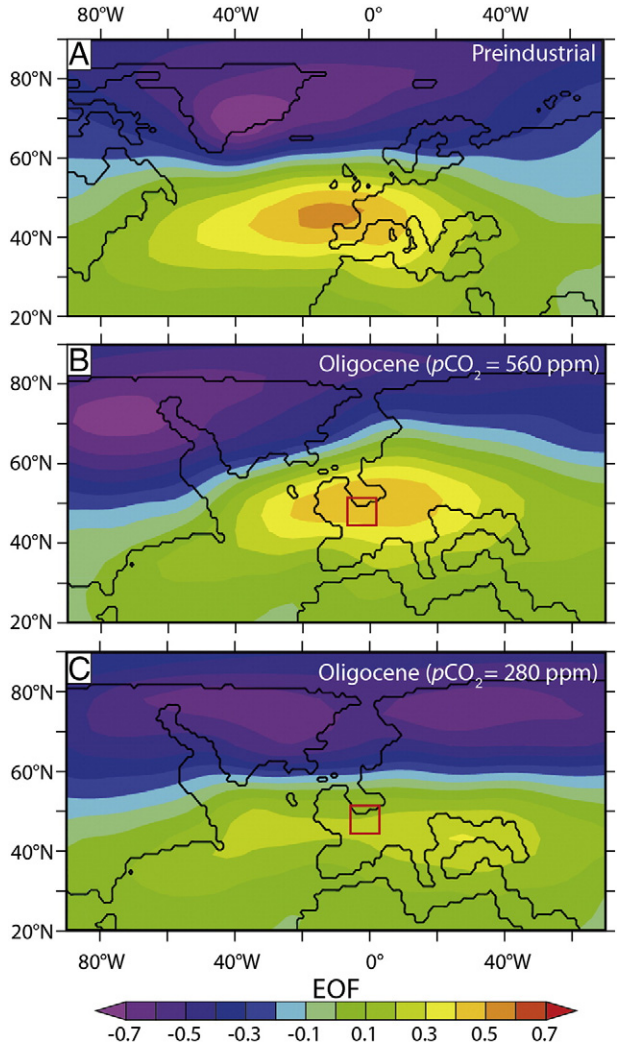

Fig. 7. The empirical orthogonal function of the modeled winter sea-level pressure across the North Atlantic sector for (A) preindustrial, (B) O-560 (Oligocene with atmospheric pCO_2 set at 560 ppm) and (C) O-280 (Oligocene with atmospheric pCO_2 set at 280 ppm) simulations. Modern-like NAO pattern (positive and a negative centers of action located at subpolar and European mid latitude, respectively) is visible in both (A) and (B).

Furthermore, the occurrence of common spectral frequencies in three different mollusk taxa covering a stratigraphic window of 5 Myr lends support to the interpretation that the observed cycles reflect a large-scale climate signal rather than local phenomena or individual physiological properties of the bivalves.

Numerical climate models support the sclerochronological interpretation and allow a characterization of atmospheric dynamics across the North Atlantic sector during the Oligocene. According to these simulations, a large scale atmospheric circulation pattern comparable to the modern NAO controlled precipitation rates across Europe during that time. The results of the CWT analysis of simulated NAO indices are coherent with those derived from the SGI_{shell} chronologies. These results further corroborate the hypothesis that an NAO precursor already existed during the Oligocene, i.e., 20 Myr earlier than previously assumed (Brachert et al., 2006).

4.1. Driving environmental factors for growth

Obtaining climate information from shell growth increments widths of bivalve mollusks can be very challenging. In fact, in order to link the life history traits of accretionary organisms to changes in atmospheric circulation requires knowledge of the environmental parameters responsible for shell growth remained unveiled. In general, the two main drivers of shell growth in bivalves are water temperature and food availability. Temperature is considered to control the metabolic rate of the bivalve (Schöne, 2008). When environmental conditions exceed the species specific range of optimum growth, shell accretion is retarded or stopped (e.g., Royer et al., 2013). However, as previously shown by Walliser et al. (2015, 2016), Oligocene glycymerids from Central Europe grew uninterruptedly during winter and summer, suggesting that temperatures remained well within the range of tolerance of these organisms.

The good correlation between the average $\delta^{13}C_{shell}$ values and growth rates (Fig. 3B) suggests that growth rate was coupled to fluctuations in food supply. Carbon incorporated into the shells of bivalves originates mainly from dissolved inorganic carbon (DIC) and to a lower extent (up to 10%) from metabolized food (e.g., McConnaughey et al., 1997; McConnaughey, 2003). In the case of filter feeding bivalves such as glycymerids the latter is mainly composed of particulate organic carbon (POC; Galap et al., 1999). Due to photosynthetic isotope fractionation effects, both the isotopic composition of the DIC and the POC can vary through time depending on the rate of primary production (e.g., Deuser et al., 1968). During times of high primary productivity, phytoplankton preferentially sequesters light carbon isotopes from the environmental DIC, which, in turn, becomes enriched in ^{13}C. For this reason, inter-annual variations of the carbon isotope composition of bivalve shells have been proposed as a potential proxy for changes in primary productivity (e.g., Lorrain et al., 2004; Poulain et al., 2010; Ivany et al., 2011; Goodwin et al., 2013).

According to the results in the present study, the incorporation of environmental carbon into the shells was also affected by ageing. The $\delta^{13}C_{shell}$ data clearly display a general trend toward lower values in all studied bivalves (Figs. 3 and 4A). Comparable $\delta^{13}C_{shell}$ trends throughout ontogeny have also been reported from modern bivalves (e.g., Lorrain et al., 2004; Gillikin et al., 2007; McConnaughey and Gillikin, 2008). Lorrain et al. (2004) argued that the isotopically light metabolic CO_2 derived from ingested food becomes increasingly relevant as a carbon source for shell production at higher ontogenetic age. The results of the present study seem to be coherent with this interpretation. Additionally, the 39-years long $\delta^{13}C_{shell}$ chronology of specimen MB-Wht-4 shows that this switch in proportion of carbon source occurred very rapidly within few a years after the age of 20th (Fig. 4). Similar drops in $\delta^{13}C_{shell}$ values are also partially visible in the other studied *G. planicostalis* shells, but at slightly different times during the ontogeny (Fig.3A). This finding may indicate a connection between the $\delta^{13}C_{shell}$ drop and processes related to the individual life history rather than to species-specific features. For example, the isotopic decline could reflect physiological related to sexual maturation.

The recognition of this $\delta^{13}C_{shell}$ drop is crucial for the interpretation of the apparently contrasting results observed in specimen MB-Wht-4 (Fig. 4B). In fact, the 39-year long data chronology from this specimen reveals a positive correlation between $\delta^{13}C_{shell}$ and age-detredend shell growth within the first 20 years of life. However, an opposite relationship was observed in later years. It is likely, that annual $\delta^{13}C_{shell}$ data during the early ontogeny reflect variations in seawater $\delta^{13}C_{DIC}$, whereas, those from later years reflect variations in the $\delta^{13}C_{POC}$ signal. Considering an average $\delta^{13}C_{POC}$ value of ca. −27‰ (e.g., Goericke and Fry, 1994) at mid latitudes, the drop in $\delta^{13}C_{shell}$ observed in the specimen MB-Wht-4 would reflect a 4% higher contribution of metabolic CO_2 to the shell carbonate. Possibly, this increase would already suffice to explain the $\delta^{13}C_{DIC}$ signal in the in the $\delta^{13}C_{shell}$ records. As mentioned before, both $\delta^{13}C_{DIC\ and}$ $\delta^{13}C_{POC}$ signals are (positively and negatively, respectively) correlated to the rate of primary productivity in the water column. Hence, the results suggest that bivalves grew their shells faster during years of higher primary production. Note, this hypothesis mainly relies on the data from of one specimen. Further studies should be conducted on modern glycymerids to test this hypothesis.

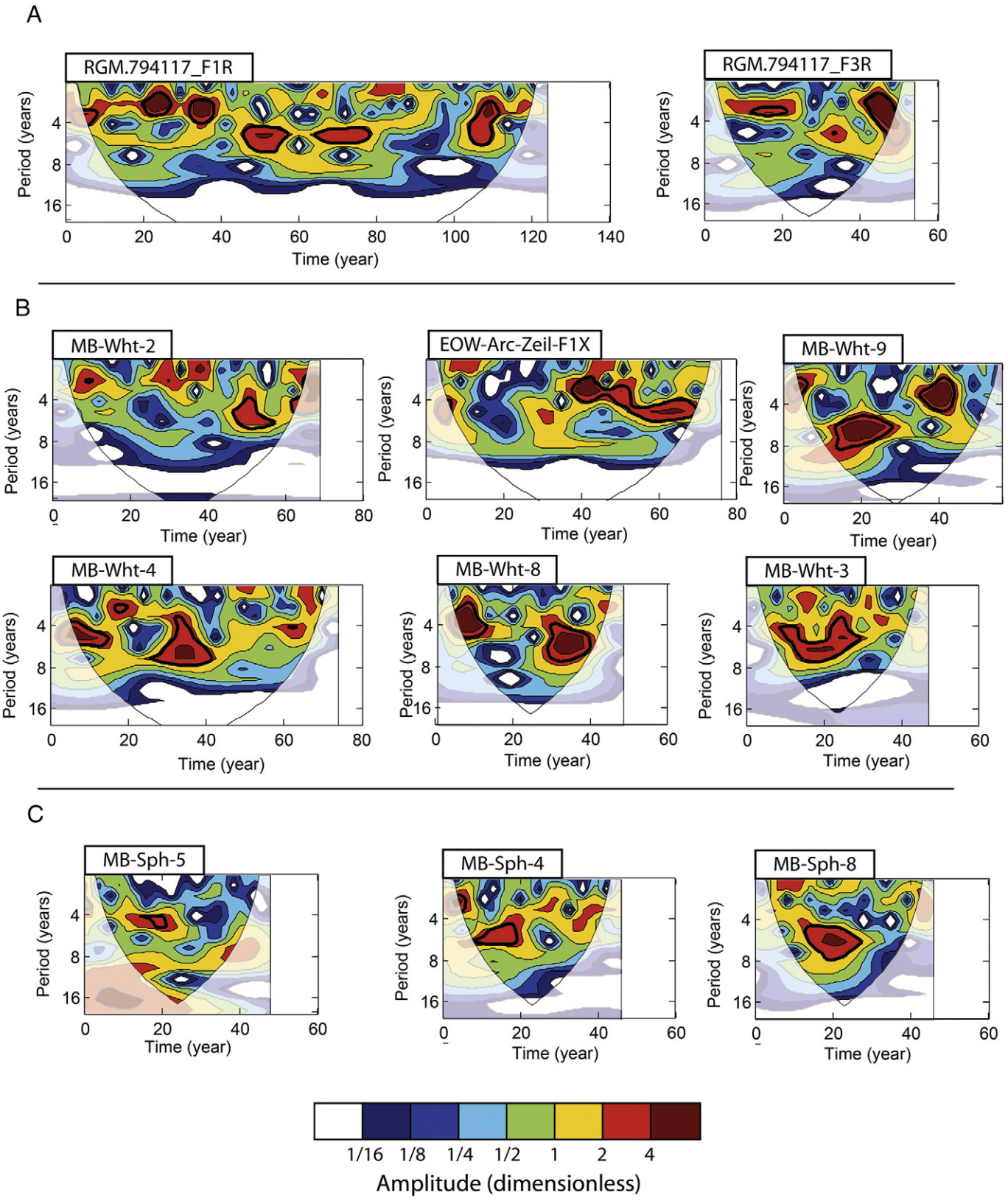

Fig. 8. Continuous wavelet spectra of the SGI_{shell} chronologies of the studied bivalve shells. (A) *Glycymeris obovata* shell from the Rupelian (early Oligocene) deposits of the Mommen sand pit near Vliermaal (Bilzen Formation, Belgium). (B) *Glycymeris planicostalis* (MB-WHT-*) and *Arctica islandica* (EOW-Arc-Zeil-F1X) shells from the Rupelian deposits of the outcrops 'Trift' and 'Zeilstück' near Weinheim (Alzey Formation, Germany). (C) *Glycymeris planicostalis* shells from the Rupelian deposits of the outcrop 'Sommersee' near Spiesheim (Stadecken Formation, Germany). Thick black contour lines display significant powers signals (above 5% significance level against red-noise spectrum). The CWT with SGI_{shell} time-series and relative growth measurement data are provided in the supplementary material.

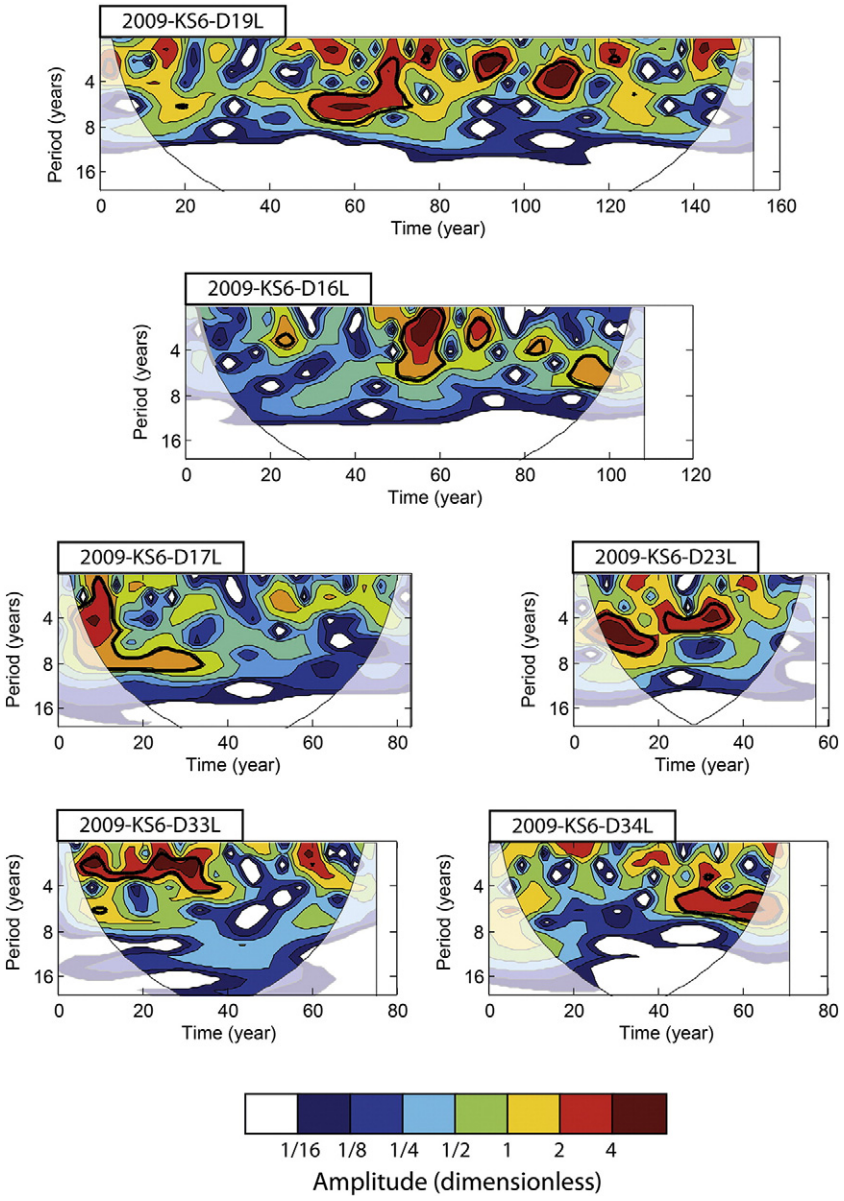

Fig. 9. Continuous wavelet spectra of the SGI_{shell} chronologies of *Glycymeris obovata* shells from the Chattian (late Oligocene) deposit of the Bergpark Wilhelmshöhe, Kassel (Kassel Formation, Germany). Thick black contour lines display significant powers signals (above 5% significance level against red-noise spectrum). The CWT with SGI_{shell} time-series and relative growth measurement data are provided in the supplementary material.

4.2. Spectral properties of SGI_{shell} chronologies

Unfortunately, it is not possible to preclude that some of the CWT spectra may bear analytical artifacts (e.g., edge effects; see CWT spectra of specimen 2009-KS-D17L; Fig. 9). However, both longer (>70 year) and shorter (<70 year) SGI_{shell} chronologies displayed significant powers between the 3 to 7-year bands (Figs. 8 and 9). This suggested that most of the high powers located between these periods are likely not the result of artifacts, but reflect oscillations of environmental conditions to which the studied bivalves were exposed.

As demonstrated by other studies of bivalves, including modern representatives of the studied taxa (e.g., Brocas et al., 2013; Schöne et al., 2003), fluctuations of environmental conditions, in particular food supply, can influence shell growth rate (Brey and Hain, 1992; Ambrose et al., 2006; Witbaard et al., 1997). However, recent studies on *Yoldia eightsi* and *Laternula elliptica* from Antarctica revealed the existence of species-specific periodical cycles in shell growth that were not related to environmental fluctuations (Román-González et al., 2017). In this regard, the authors suggested as possible explanation the presence of physiological rhythms related to energy reallocation during gametogenesis. It remains unknown if similar physiological cycles governed the growth of the studied shells, and no such information have been reported for the modern relatives of the *Glycymeris* and *Arctica* species. However, if the periodic signals observed in the SGI chronologies were related to physiological processes, one would expect more persistent power signals in the CWT at certain periods. This is not the case in the present study, because the CWT analysis revealed non-stationary signals and significant powers in all different species (Figs. 8 and 9).

Since the studied fossils cover a stratigraphic range of about 5 Myr (30–25 Ma) and originate from different marine basins located several hundreds of km away from each other we hypothesize that the observed common signals are not merely the results of local environmental fluctuations but rather reflect a common large-scale climate phenomenon. Furthermore, the reconstructed seasonal growth rates

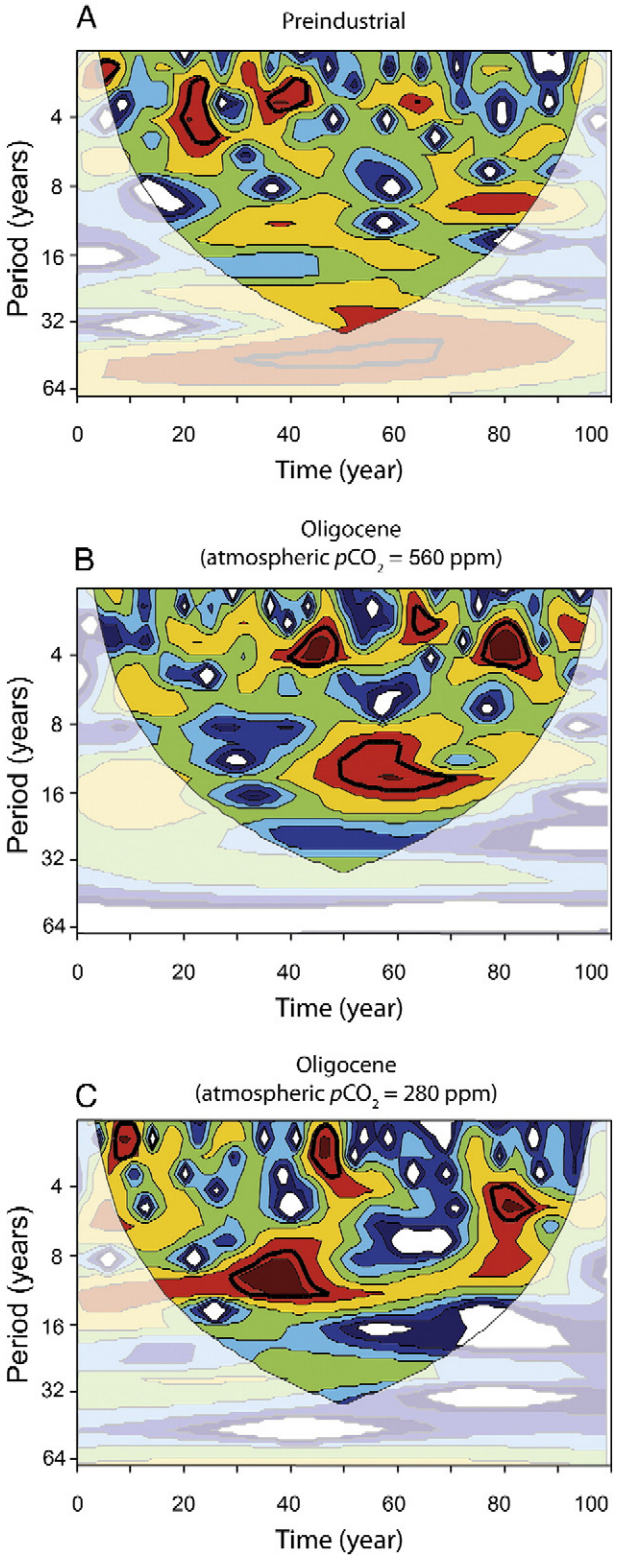

Fig. 10. Continuous wavelet spectra of the simulated NAO indices. Computed from the (A) preindustrial, (B) O-560 (Oligocene with atmospheric pCO_2 set at 560 ppm) and (C) O-280 (Oligocene with atmospheric pCO_2 set at 280 ppm) climate simulations. Thick black contour lines display significant powers (above 5% significance level against red-noise spectrum).

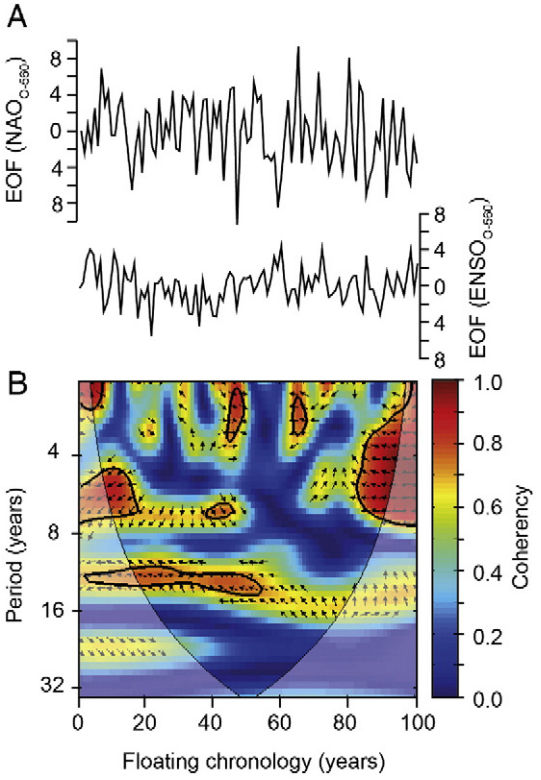

Fig. 11. Time-series of the simulated ENSO and NAO indices and their wavelet coherence. (A) Time-series of the leading PC1 of the EOF were used to define the NAO (upper panel) and ENSO (lower panel) in the Oligocene simulation with pCO_2 set at 560 ppm (O-560). (B) Wavelet coherence and relative phase relationships between the time-series showed in (A). Phase arrows pointing to the right = in-phase, pointing to the left = anti-phase, down/up = phase lag. Thick contour indicates the 5% significance level against red-noise.

revealed that glycymerids grew largely during the winter months (Fig. 5), the season during which climate variability in central Europe is typically strongest. A similar growing season was observed in the Oligocene *Arctica islandica* (Walliser et al., 2016). According to the reconstructions, this phenomenon could be compatible with a large-scale atmospheric circulation pattern. This hypothesis is further corroborated by the observed non-stationarity of the spectral powers (Figs. 8 and 9).

4.3. Characterization of the inter-annual climate pattern

Atmospheric circulation exerts a dominant influence on coastal environments by controlling seasonal temperatures, wind stress, and hydrological cycles on land and ultimately primary production rates in coastal environments (e.g., Lindahl et al., 1998; Ottersen et al., 2001; Hanna et al., 2006). Hence, it is very likely that the observed variations of growth increment widths reflect Oligocene climate dynamics. According to previous studies changes in phytoplankton dynamics in the studied marine basins were primarily induced by variations in precipitation rate (Pross, 2001; Pross and Schmiedl, 2002), which, according to our simulations, were controlled by atmospheric circulation, i.e. wSLP changes (Fig. 6C). Most likely, the studied bivalves recorded such changes in their shells in the form of annual increment widths that fluctuated on quasi-decadal time-scales.

CWT analysis revealed significant powers mainly around the 3 to 7-year band (Figs. 8 and 9). The presence of similar cycles in other fossil archives has been often considered to be indicative of ENSO (e.g., Mingram, 1998; Lenz et al., 2010; Galeotti et al., 2010; Davies et al., 2011), which exhibits 2 to 7-years oscillations (Rasmusson et al., 1990). However, at least for the Miocene epoch this interpretation is questioned by other works. For example, annually resolved $\delta^{18}O$ records of fossil corals from Greece exhibited periodic oscillations between 2

and 5 years and were interpreted to reflect NAO variability (Brachert et al., 2006; Mertz-Kraus et al., 2009). Particularly, Brachert et al. (2006) provided numerical climate model data which indicated a wSLP distribution across the North Atlantic resembling the present-day situation. A similar configuration is also observed in our climate model data and the distribution of the wSLP-EOF domains across the North Atlantic in the O_{560} simulation support the existence of an NAO-like pattern (Fig. 7). In this regard, it is likely that the formation and the distribution of the SLP seesaw (the engine of the NAO; Hurrell and Deser, 2009) largely depended on the size on the North Atlantic basin northern hemisphere during the Oligocene. In fact, the paleogeographical distribution of continents in regulating climate dynamics has also been shown for ocean heat transport patterns (e.g., Bice et al., 2000). Therefore, the coexistence of the ENSO and the NAO as it happens today, cannot be exclude a priori for past time intervals, neither the Miocene nor the Oligocene itself.

The question remained which climate phenomenon is registered in the spectral properties of the SGI_{shell} data if both ENSO and a proto-NAO coexisted during the Oligocene. The presence of ENSO-driven inter-annual climate dynamics in Europe has often been associated with greenhouse intervals in earth history, e.g., the Eocene (Lenz et al., 2010) or the Miocene (Galeotti et al., 2010). According to these reconstructions, higher global temperatures would increase the strength of the ENSO, resulting in perturbated global climate patterns. A similar scenario has been suggested by climate projections for a warmer future world (e.g., Cai et al., 2014). The extent of the teleconnection between the Oligocene ENSO and NAO can be explored by evaluating the coherence between the CWT of the two simulated circulation patterns (e.g., Grinsted et al., 2004). Our results however, indicate ambiguous coherence between the simulated indices in the 3–7-year band. In fact, if the modeled phenomena were teleconnected, phase arrows in the significant areas, should have pointed in the same direction for a given wavelength (Fig. 11). As this is not the case, teleconnection of the two patterns was likely reduced, if not absent. In a geological context this is not surprising, since the Oligocene epoch was an icehouse interval (e.g., Miller et al., 1991).

Unfortunately, coherency between CWT of different SGI_{shell} chronologies or between the SGI_{shell} chronologies and the simulated ENSO or NAO indices cannot be tested, because, the coherency test requires calendar dated the time-series. In other words, to apply this method, it must be assumed that the studied shells grew during the exact same time. This was very likely not the case, and any coherent pattern revealed by the cross-wavelet analysis would be the result of randomness. The absence of an applicable statistical method for the evaluation of coherence between fossil, modeled and observational time-series makes the interpretation of the wavelet transforms difficult. Usually, the recognition of the ENSO rhythm in annually-resolved fossil records is based on a qualitative assessment of the spectrogram signals (Galeotti et al., 2010; Davies et al., 2011). For example, Galeotti et al. (2010) argued that cycles observed in the halovarves from Italy were more stationary and sustained than those observed in the inter-annual frequencies of the modern NAO, and therefore were interpreted to reflect an ENSO signal. Accordingly, the strong non-stationary nature of the power spectra of the Oligocene bivalves lends support to the interpretation of the CWT_{SGI} signal as reflecting an NAO-like variability. This interpretation would also be coherent with the presence of significant CWT_{SGI} powers of the outside the typical range of the ENSO, i.e., 8–12 years. Interestingly, periodicities at longer wavelengths were also identified in the wavelet transforms of the $NAO_{O\text{-}560}$ simulation (8–16 years), and are also known to occur also in the modern NAO (Jevrejeva et al., 2003).

Similarity between spectrograms from proxy data, climate model simulations and modern observational data, however, should be considered carefully, because each data set entails limitations related to the different time scale under consideration. The climate model in this study considers a 5 Myr-long time interval and provides a 100 year-long simulated chronology. Although, no major global paleotectonic or climatic reorganization took place during the studied time interval (e.g., Markwick, 2007), the results of the simulation are only broadly indicative for the actual variability in the North Atlantic during the Oligocene. Therefore, possible fluctuations outside the revealed wavelengths in the $NAO_{O\text{-}560}$ band should be take into account and the comparison to proxy data should be performed considering the results from all specimens together and not each single shell individually. In fact, reconstructions of the NAO variability over the past millennium (e.g., Trouet et al., 2009; Holland et al., 2014; Ortega et al., 2015; Reynolds et al., 2017) show non-stationary signals, i.e., rhythmic oscillations of this atmospheric pattern changed over longer time intervals. According to these studies such changes are likely related to the impact of external forcing, such as generally increasing temperatures during the Medieval Climate Anomaly (Trouet et al., 2009; Holland et al., 2014) or volcanic eruptions (Ortega et al., 2015). In this regard, CWT analysis on the reconstructed NAO index of Ortega et al. (2015; see Supplementary data) reveals shifts in the wavelengths, the duration and the density of relevant (above 5% significance) signals over the past centuries. Hence, it is likely that similar events took also place during the Oligocene. Although, the studied chronologies provide relatively short time windows, the large sample size ($n = 17$) of the SGI data provides hints that the Oligocene atmospheric circulation pattern also possessed a certain degree of variability through time. For example, more sustained CWT_{SGI} signals are revealed in the chronologies of specimens EOW-Arc-Zeil-F1X (Fig. 9) and 2009-KS6-D17L, whereas, shorter signals are visible in RGM.794117_F1R, 2009-KS6-D19L and 2009-KS6-D19L (Figs. 9 and 10). This further supports the hypothesis of an NAO rather than an ENSO rhythm influencing the inter-annual changes of Oligocene climate in Central Europe. In fact, proxy based and numerical climate model data suggest that the year-to-year variability remained more or less stable since the Cretaceous (e.g., Huber and Caballero, 2003; Galeotti et al., 2010; Lenz et al., 2010; Batenburg et al., 2011; Davies et al., 2011; Ivany et al., 2011).

4.4. Differences between the Oligocene NAO-like pattern and the modern NAO

The similarities between the spectral peaks of the SGI_{shell} and the $NAO_{O\text{-}560}$ time-series support the interpretation that a proto NAO-like pattern influenced the climate variability on Central Europe during the Oligocene. According to the CWT results, however, the main quasi-decadal atmospheric variability during the Oligocene (3–7 years) differed from the time-scales of the modern NAO (i.e., biennial and 6–10 year cycles; Hurrell and Van Loon, 1997). This is probably associated with the different spatial distribution of the two patterns related to different paleogeographical settings of the studied time intervals (Fig. 7). The Oligocene atmospheric variability compares well to inter-annual oscillations observed in high-resolution records of Miocene age from Europe (Brachert et al., 2006; Mertz-Kraus et al., 2009). Similarly to the Oligocene, the Miocene was an epoch characterized by a narrower North Atlantic Basin than present and a reduced Greenland ice sheet (Markwick, 2007). The westward displacement of the $NAO_{O\text{-}560}$ pattern likely resulted from higher atmospheric pCO_2 levels during the Oligocene. In fact, the two Oligocene simulations yielded markedly different EOF-wSLP configurations. Stronger atmospheric forcing ($O\text{-}560_{sim}$) resulted in a counterclockwise rotation of the EOF pattern (Fig. 7B and C). This is likely because higher global temperatures induce a northward migration of the sub-tropical jet streams which ultimately results in the contraction of the Northern Hemispheric atmospheric circulation patterns (Archer & Caldeira, 2008; Frauenfeld & Davis, 2003).

As suggested by the results, the North Atlantic variability gained control on the short-term climate fluctuations of Central Europe as early as during the Oligocene. Prior to that time, the climate of this region was influenced by the ENSO (Mingram, 1998; Lenz et al., 2010). The present study represents the first attempt to investigate the transition from an ENSO-dominated climate regime to an NAO-like climate regime in Central Europe. Based on the data provided here, future

studies should further explore if the emerging NAO-like pattern has contributed to the pervasive climate deterioration near the Eocene/Oligocene boundary (e.g., Ivany et al., 2000; Eldrett et al., 2009) and its possible role in the Late Paleogene terrestrial and marine faunal turnover (e.g., Prothero, 1994; Prothero et al., 2003).

5. Conclusions

The present study represents the first attempt to characterize the inter-annual climate variability of Central Europe during the Oligocene by combining proxy data and numerical climate models. Stable carbon isotope records of Oligocene glycymerids bivalves indicate that shell growth rates were likely regulated by food availability (primary production) in the water column. The spectral properties of the annual shell growth time-series of Oligocene bivalves from Central Europe revealed cycles at 2–12 years, and particularly within the mostly concentrated within the 3 to 7-year band, closely resembling the variability of modern atmospheric circulation patterns. It is discussed here whether the signals represents an ENSO or an NAO-like pattern. Although a contribution of ENSO cannot be completely precluded, the combination of shell data and climate model simulation data provides arguments for the existence of a proto NAO-like pattern across the North Atlantic already during the Oligocene. According to numerical climate simulations, the spatial distribution and internal variability of the NAO-like pattern slightly differed from today, due to the peculiar paleogeography and higher atmospheric pCO_2 concentrations during the Oligocene. Accordingly, the new data presented here show that an NAO-like atmospheric circulation pattern already existed during the middle Oligocene (31–25 Ma), about 20 Myr earlier than previously documented. Further studies are needed to better characterize the relationship between annual growth rates and primary production rates, as well as to explore the variability of the NAO-like pattern and its connection to the Central Pacific during the Oligocene.

Acknowledgments

We gratefully acknowledge the help of Michael Maus during isotope analysis and Christoph Füllenbach for his assistance during fieldwork. Furthermore, we thank the Naturalis Biodiversity Center of the National Museum of Natural History of The Netherlands for providing the material from Belgium. Funding for this study was kindly provided by the German Research Foundation, DFG (SCHO 793/11) to BRS, the National Center of Science, Poland (DEC-2012/07/N/ST10/03419) and the DAAD (2015/16, 57130104) to IN, as well as the Helmholtz society (PACES program Topic 3WP2) to GL.

Appendix A. Supplementary data

Supplementary data to this article can be found online at http://dx.doi.org/10.1016/j.palaeo.2017.03.020.

References

Abelmann, A., Gersonde, R., Knorr, G., Zhang, X., Chapligin, B., Maier, E., Esper, O., Friedrichsen, H., Lohmann, G., Meyer, H., Tiedemann, R., 2015. The seasonal sea ice zone in the glacial Southern Ocean as a carbon sink. Nat. Commun. 6:8136. http://dx.doi.org/10.1038/ncomms9136.

Ambrose, W.G., Caroll, M.L., Greenacre, M., Thorrold, S.R., McMahon, K.W., 2006. Variation in *Serripes groenlandicus* (Bivalvia) growth in a Norwegian high-Arctic fjord: evidence for local- and large-scale climatic forcing. Glob. Chang. Biol. 12:1595–1607. http://dx.doi.org/10.1111/j.1365-2486.2006.01181.x.

Archer, C.L., Caldeira, K., 2008. Historical trends in the jet streams. Geophys. Res. Lett. 35, L08803. http://dx.doi.org/10.1029/2008GL033614.

Bakker, P., Masson-Delmotte, V., Martrat, B., Charbit, S., Renssen, H., Groger, M., Krebs-Kanzow, U., Lohmann, G., Lunt, D.J., Pfeiffer, M., Phipps, S.J., Prange, M., Ritz, S.P., Schulz, M., Stenni, B., Stone, E.J., Varma, V., 2014. Temperature trends during the present and last interglacial periods - a multi-model-data comparison. Quat. Sci. Rev. 99: 224–243. http://dx.doi.org/10.1016/j.quascirev.2014.06.031.

Batenburg, S.J., Reichart, G.J., Jilbert, T., Janse, M., Wesselingh, F.P., Renema, W., 2011. Interannual climate variability in the Miocene: high resolution trace element and stable isotope ratios in giant clams. Palaeogeogr. Palaeoclimatol. Palaeoecol. 306:75–81. http://dx.doi.org/10.1016/j.palaeo.2011.03.031.

Berger, J.-P., Reichenbacher, B., Becker, D., Grimm, M.C., Grimm, K.I., Picot, L., Storni, A., Pirkenseer, C., Derer, C., Schaefer, A., 2005a. Paleogeography of the Upper Rhine Graben (URG) and the Swiss Molasse Basin (SMB) from Eocene to Pliocene. Int. J. Earth Sci. 94:697–710. http://dx.doi.org/10.1007/s00531-005-0475-2.

Berger, J.-P., Reichenbacher, B., Becker, D., Grimm, M.C., Grimm, K.I., Picot, L., Storni, A., Pirkenseer, C., Schaefer, A., 2005b. Eocene-Pliocene time scale and stratigraphy of the Upper Rhine Graben (URG) and the Swiss Molasse Basin (SMB). Int. J. Earth Sci. 94:711–731. http://dx.doi.org/10.1007/s00531-005-0479-y.

Bice, K.L., Scotese, C.R., Seidov, D., Barron, E.J., 2000. Quantifying the role of geographic change in Cenozoic ocean heat transport using uncoupled atmosphere and ocean models. Palaeogeogr. Palaeoclimatol. Palaeoecol. 161:295–310. http://dx.doi.org/10.1016/S0031-0182(00)00072-9.

Black, B.A., Gillespie, D.C., MacLellan, S.E., Hand, C.M., 2008. Establishing highly accurate production-age data using the tree-ring technique of crossdating: a case study for Pacific geoduck (*Panopea abrupta*). Can. J. Fish. Aquat. Sci. 65:2572–2578. http://dx.doi.org/10.1139/F08-158.

Brachert, T.C., Reuter, M., Felis, T., Kroeger, K., Lohmann, G., Micheels, A., Fassoulas, C., 2006. *Porites* corals from Crete (Greece) open a window into Late Miocene (10 Ma) seasonal and interannual climate variability. Earth Planet. Sci. Lett. 245:81–94. http://dx.doi.org/10.1016/j.epsl.2006.03.005.

Brey, T., Hain, S., 1992. Growth, reproduction and production of *Lissarca notorcadensis* (Bivalvia, Philobryidae) in the Weddell Sea, Antarctica. Mar. Ecol. Prog. Ser. 82, 219–226.

Brocas, W.M., Reynolds, D.J., Butler, P.G., Richardson, C.A., Scourse, J.D., Ridgway, I.D., Ramsay, K., 2013. The dog cockle, *Glycymeris glycymeris* (L.), a new annually-resolved sclerochronological archive for the Irish Sea. Palaeogeogr. Palaeoclimatol. Palaeoecol. 373:133–140. http://dx.doi.org/10.1016/j.palaeo.2012.03.030.

Butler, P.G., Wanamaker, A.D., Scourse, J.D., Richardson, C.A., Reynolds, D.J., 2013. Variability of marine climate on the North Icelandic Shelf in a 1357-year proxy archive based on growth increments in the bivalve *Arctica islandica*. Palaeogeogr. Palaeoclimatol. Palaeoecol. 373:141–151. http://dx.doi.org/10.1016/j.palaeo.2012.01.016.

Cai, W., Borlace, S., Lengaigne, M., van Rensch, P., Collins, M., Vecchi, G., Timmermann, A., Santoso, A., McPhaden, M.J., Wu, L., England, M.H., Wang, G., Guilyardi, E., Jin, F.-F., 2014. Increasing frequency of extreme El Niño events due to greenhouse warming. Nat. Clim. Chang. 4:111–116. http://dx.doi.org/10.1038/nclimate2100.

Checa, A., 2000. A new model for periostracum and shell formation in Unionidae (Bivalvia, Mollusca). Tissue Cell 32:405–416. http://dx.doi.org/10.1054/tice.2000.0129.

Clark, G.R., 1974. Growth lines in invertebrate skeletons. Annu. Rev. Earth Planet. Sci. 2: 77–99. http://dx.doi.org/10.1146/annurev.ea.02.050174.000453.

Davies, A., Kemp, A.E.S., Pälike, H., 2011. Tropical ocean-atmosphere controls on inter-annual climate variability in the Cretaceous Arctic. Geophys. Res. Lett. 38:L03706. http://dx.doi.org/10.1029/2010gl046151.

Dettman, D.L., Reische, A.K., Lohmann, K.C., 1999. Controls on the stable isotope composition of seasonal growth bands in aragonitic fresh-water bivalves (unionidae). Geochim. Cosmochim. Acta 63:1049–1057. http://dx.doi.org/10.1016/S0016-7037(99)00020-4.

Deuser, W.G., Degens, E.T., Guillard, R.R.L., 1968. Carbon isotope relationships between plankton and sea water. Geochim. Cosmochim. Acta 32:657–660. http://dx.doi.org/10.1016/0016-7037(68)90055-0.

Dowsett, H.J., Foley, K.M., Stoll, D.K., Chandler, M.a., Sohl, L.E., Bentsen, M., Otto-Bliesner, B.L., Bragg, F.J., Chan, W.-L., Contoux, C., Dolan, A.M., Haywood, A.M., Jonas, J.a., Jost, A., Kamae, Y., Lohmann, G., Lunt, D.J., Nisancioglu, K.H., Abe-Ouchi, A., Ramstein, G., Riesselman, C.R., Robinson, M.M., Rosenbloom, N.a., Salzmann, U., Stepanek, C., Strother, S.L., Ueda, H., Yan, Q., Zhang, Z., 2013. Sea surface temperature of the mid-Piacenzian ocean: a data-model comparison. Sci. Rep. 3. http://dx.doi.org/10.1038/srep02013.

Eldrett, J.S., Greenwood, D.R., Harding, I.C., Huber, M., 2009. Increased seasonality through the Eocene to Oligocene transition in northern high latitudes. Nature 459:969–973. http://dx.doi.org/10.1038/nature08069.

Erdei, B., Utescher, T., Hably, L., Tamás, J., Roth-Nebelsick, A., Grein, M., 2012. Early Oligocene continental climate of the Palaeogene Basin (Hungary and Slovenia) and the surrounding area. Turk. J. Earth Sci. 21:153–186. http://dx.doi.org/10.3906/yer-1005-29.

Felis, T., Giry, C., Scholz, D., Lohmann, G., Pfeiffer, M., Pätzold, J., Kölling, M., Scheffers, S.R., 2015. Tropical Atlantic temperature seasonality at the end of the last interglacial. Nat. Commun. 6:6159. http://dx.doi.org/10.1038/ncomms7159.

Frauenfeld, O.W., Davis, R.E., 2003. Northern Hemisphere circumpolar vortex trends and climate change implications. J. Geophys. Res. 108:4423. http://dx.doi.org/10.1029/2002JD002958.

Galap, C., Netchitäilo, P., Leboulenger, F., Grillot, J.-P., 1999. Variations of fatty acid contents in selected tissues of the female dog cockle (*Glycymeris glycymeris* L., Mollusca, Bivalvia) during the annual cycle. Comp. Biochem. Physiol. A Mol. Integr. Physiol. 122: 241–254. http://dx.doi.org/10.1016/S1095-6433(99)00006-9.

Galeotti, S., von der Heydt, A., Huber, M., Bice, D., Dijkstra, H., Jilbert, T., Lanci, L., Reichart, G.J., 2010. Evidence for active El Niño Southern Oscillation variability in the Late Miocene greenhouse climate. Geology 38:419–422. http://dx.doi.org/10.1130/G30629.1.

McConnaughey, T.A., Gillikin, D.P., 2008. Carbon isotopes in mollusk shell carbonates. Geo-Mar. Lett. 28:287–299. http://dx.doi.org/10.1007/s00367-008-0116-4.

Gillikin, D.P., Lorrain, A., Meng, L., Dehairs, F., 2007. A large metabolic carbon contribution to the $\delta^{13}C$ record in marine aragonitic bivalve shells. Geochim. Cosmochim. Acta 71: 2936–2946. http://dx.doi.org/10.1016/j.gca.2007.04.003.

Goericke, R., Fry, B., 1994. Variations of marine plankton $\delta^{13}C$ with latitude, temperature, and dissolved CO_2 in the world ocean. Glob. Biogeochem. Cycles 8:85–90. http://dx.doi.org/10.1029/93GB03272.

Goodwin, D.H., Gillikin, D.P., Roopnarine, P.D., 2013. Preliminary evaluation of potential stable isotope and trace element productivity proxies in the oyster *Crassostrea gigas*. Palaeogeogr. Palaeoclimatol. Palaeoecol. 373:88–97. http://dx.doi.org/10.1016/j.palaeo.2012.03.034.

Grimm, K.I., Grimm, M., Radtke, G., Kadolsky, D., Schäfer, P., Franzen, J.L., Schindler, T., Hottenrott, M., 2011. Mainzer Becken. Schriftenreihe der Deutschen Gesellschaft für Geowissenschaften 75, 133–209.

Grinsted, A., Moore, J.C., Jevrejeva, S., 2004. Application of the cross wavelet transform and wavelet coherence to geophysical time series. Nonlinear Process. Geophys. 11: 561–566. http://dx.doi.org/10.5194/npg-11-561-2004.

Grossman, E.L., Ku, T.-L., 1986. Oxygen and carbon isotope fractionation in biogenic aragonite: temperature effects. Chem. Geol. Isot. Geosci. 59:59–74. http://dx.doi.org/10.1016/0168-9622(86)90057-6.

Hagemann, S., Dümenil, L., 1998. A parametrization of the lateral waterflow for the global scale. Clim. Dyn. 14:17–31. http://dx.doi.org/10.1007/s003820050205.

Hanna, E., Jónsson, T., Ólafsson, J., Valdimarsson, H., 2006. Icelandic coastal sea surface temperature records constructed: putting the pulse on air-sea-climate interactions in the northern North Atlantic. Part I: comparison with HadISST1 open-ocean surface temperatures and preliminary analysis of long-term pattern. J. Clim. 19:5652–5666. http://dx.doi.org/10.1175/JCLI3933.1.

Haq, B.U., Hardenbol, J., Vail, P.R., 1988. Mesozoic and Cenozoic chronostratigraphy and cycles of sea-level change. In: Wilgus, C.K., Hasting, B.S., Posamentier, H., Van Wagoner, J., Ross, C.K., Kendall, C.G.S.C. (Eds.), Mesozoic and Cenozoic Sequence Stratigraphy of European Basins. SEPM Special Publications vol. 42:pp. 71–108. http://dx.doi.org/10.2110/pec.88.01.0071.

Haywood, A.M., Hill, D.J., Dolan, A.M., Otto-Bliesner, B.L., Bragg, F., Chan, W.L., Chandler, M.A., Contoux, C., Dowsett, H.J., Jost, A., Kamae, Y., Lohmann, G., Lunt, D.J., Abe-Ouchi, A., Pickering, S.J., Ramstein, G., Rosenbloom, N.A., Salzmann, U., Sohl, L., Stepanek, C., Ueda, H., Yan, Q., Zhang, Z., 2013. Large-scale features of Pliocene climate: results from the Pliocene Model Intercomparison Project. Clim. Past 9: 191–209. http://dx.doi.org/10.5194/cp-9-191-2013.

Henderiks, J., Pagani, M., 2008. Coccolithophore cell size and the Paleogene decline in atmospheric CO_2. Earth Planet. Sci. Lett. 269:576–584. http://dx.doi.org/10.1016/j.epsl.2008.03.016.

Héran, M.-A., Lécuyer, C., Legendre, S., 2010. Cenozoic long-term terrestrial climatic evolution in Germany tracked by $\delta^{18}O$ of rodent tooth phosphate. Palaeogeogr. Palaeoclimatol. Palaeoecol. 285:331–342. http://dx.doi.org/10.1016/j.palaeo.2009.11.030.

Holland, H.A., Schone, B.R., Lipowsky, C., Esper, J., 2014. Decadal climate variability of the North Sea during the last millennium reconstructed from bivalve shells (*Arctica islandica*). The Holocene 24:771–786. http://dx.doi.org/10.1177/0959683614530438.

Huber, M., Caballero, R., 2003. Eocene El Niño: evidence for robust tropical dynamics in the "hothouse". Science 299:877–881. http://dx.doi.org/10.1126/science.1078766.

Hurrell, J.W., 1995. Decadal trends in the North Atlantic Oscillation: regional temperatures and precipitation. Science 269:676–679. http://dx.doi.org/10.1126/science.269.5224.676.

Hurrell, J.W., Deser, C., 2009. North Atlantic climate variability: the role of the North Atlantic Oscillation. J. Mar. Syst. 78:28–41. http://dx.doi.org/10.1016/j.jmarsys.2008.11.026.

Hurrell, J.W., Van Loon, H., 1997. Decadal variations in climate associated with the North Atlantic Oscillation. Clim. Chang. 36:301–326. http://dx.doi.org/10.1007/978-94-015-8905-5_4.

Ivany, L.C., 2012. Reconstructing paleoseasonality from accretionary skeletal carbonates - challenges and opportunities. In: Ivany, L.C., Huber, B.T. (Eds.), Reconstructing Earth's Deep-time Climate - The State of the Art. Paleontological Society Short Course, pp. 133–165.

Ivany, L.C., Patterson, W.P., Lohmann, K.C., 2000. Cooler winters as a possible cause of mass extinctions at the Eocene/Oligocene boundary. Nature 407:887–890. http://dx.doi.org/10.1038/35038044.

Ivany, L.C., Brey, T., Huber, M., Buick, D.P., Schöne, B.R., 2011. El Niño in the Eocene greenhouse recorded by fossil bivalves and wood from Antarctica. Geophys. Res. Lett. 38: L16709. http://dx.doi.org/10.1029/2011GL048635.

Jevrejeva, S., Moore, J.C., Grinsted, A., 2003. Influence of the Arctic Oscillation and El Niño-Southern Oscillation (ENSO) on ice conditions in the Baltic Sea: the wavelet approach. J. Geophys. Res. 108:4677. http://dx.doi.org/10.1029/2003JD003417.

Jungclaus, J.H., Keenlyside, N., Botzet, M., Haak, H., Luo, J.J., Latif, M., Marotzke, J., Mikolajewicz, U., Roeckner, E., 2006. Ocean circulation and tropical variability in the coupled model ECHAM5/MPI-OM. J. Clim. 19:3952–3972. http://dx.doi.org/10.1175/JCLI3827.1.

Kageyama, M., Merkel, U., Otto-Bliesner, B., Prange, M., Abe-Ouchi, A., Lohmann, G., Roche, D.M., Singarayer, J., Swingedouw, D., Zhang, X., 2012. Climatic impacts of fresh water hosing under Last Glacial Maximum conditions: a multi-model study. Clim. Past 9: 935–953. http://dx.doi.org/10.5194/cp-9-935-2013.

Kloosterboer-Van Hoeve, M.L., Steenbrink, J., Visscher, H., Brinkhuis, H., 2006. Millennial-scale climatic cycles in the Early Pliocene pollen record of Ptolemais, northern Greece. Palaeogeogr. Palaeoclimatol. Palaeoecol. 229:321–334. http://dx.doi.org/10.1016/j.palaeo.2005.07.002.

Knorr, G., Lohmann, G., 2014. Climate warming during Antarctic ice sheet expansion at the Middle Miocene transition. Nat. Geosci. 7:376–381. http://dx.doi.org/10.1038/ngeo2119.

Knorr, G., Butzin, M., Micheels, A., Lohmann, G., 2011. A warm Miocene climate at low atmospheric CO_2 levels. Geophys. Res. Lett. 38:1–5. http://dx.doi.org/10.1029/2011GL048873.

Kocsis, L., Ozsvárt, P., Becker, D., Ziegler, R., Scherler, L., Codrea, V., 2014. Orogeny forced terrestrial climate variation during the late Eocene-early Oligocene in Europe. Geology 42:727–730. http://dx.doi.org/10.1130/G35673.1.

Kuhlemann, J., 2007. Paleogeographic and paleotopographic evolution of the Swiss and Eastern Alps since the Oligocene. Glob. Planet. Chang. 58:224–236. http://dx.doi.org/10.1016/j.gloplacha.2007.03.007.

Lenz, O.K., Wilde, V., Riegel, W., Harms, F.-J., 2010. A 600 k.y. record of El Niño–Southern Oscillation (ENSO): evidence for persisting teleconnections during the Middle Eocene greenhouse climate of Central Europe. Geology 38:627–630. http://dx.doi.org/10.1130/G30889.1.

Lindahl, O., Belgrano, A., Davidsson, L., Hernroth, B., 1998. Primary production, climatic oscillations, and physico-chemical processes: the Gullmar Fjord time-series data set (1985-1996). ICES J. Mar. Sci. 55:723–729. http://dx.doi.org/10.1006/jmsc.1998.0379.

Lohmann, G., Pfeiffer, M., Laepple, T., Leduc, G., Kim, J.H., 2013. A model-data comparison of the Holocene global sea surface temperature evolution. Clim. Past 9:1807–1839. http://dx.doi.org/10.5194/cp-9-1807-2013.

Lorrain, A., Paulet, Y.-M., Chauvaud, L., Dunbar, R., Mucciarone, D., Fontugne, M., 2004. $\delta^{13}C$ variation in scallop shells: increasing metabolic carbon contribution with body size? Geochim. Cosmochim. Acta 68:3509–3519. http://dx.doi.org/10.1016/j.gca.2004.01.025.

Lott, F., Miller, M.J., 1997. A new subgrid-scale orographic drag parametrization: its formulation and testing. Q. J. R. Meteorol. Soc. 123:101–127. http://dx.doi.org/10.1002/qj.49712353704.

Lunt, D.J., Abe-Ouchi, A., Bakker, P., Berger, A., Braconnot, P., Charbit, S., Fischer, N., Herold, N., Jungclaus, J.H., Khon, V.C., Krebs-Kanzow, U., Langebroek, P.M., Lohmann, G., Otto-Bliesner, B., Park, W., Pfeiffer, M., Phipps, S.J., Prange, M., Rachmayani, R., Renssen, H., Rosenbloom, N., Schneider, B., Stone, E.J., Takahashi, K., Wei, W., Yin, Q., Zhang, Z.S., 2013. A multi-model assessment of Last interglacial temperatures. Clim. Past 9: 699–717. http://dx.doi.org/10.5194/cp-9-699-2013.

Marchitto, T.M., Jones, G.A., Goodfriend, G.A., Weidman, C.R., 2000. Precise temporal correlation of Holocene mollusk shells using sclerochronology. Quat. Res. 53:236–246. http://dx.doi.org/10.1006/qres.1999.2107.

Markwick, P.J., 2007. The palaeogeographic and palaeoclimatic significance of climate proxies for data-model comparisons. In: Williams, A., Haywood, A.M., Gregory, F.J., Schmidt, D.N. (Eds.), Deep-time Perspectives on Climate Change: Marrying the Signal from Computer Models and Biological Proxies. Geological Society London, London, pp. 251–312.

Marsland, S.J., Haak, H., Jungclaus, J.H., Latif, M., Röske, F., 2003. The Max-Planck-Institute global ocean/sea ice model with orthogonal curvilinear coordinates. Ocean Model 5: 91–127. http://dx.doi.org/10.1016/S1463-5003(02)00015-X.

Martini, E., 1982. Bestandsaufnahme des Nannoplankton im "prä-aquitanen" Tertiär des Mainzer Beckens. Mainz. Geowiss. Mitt. 10, 29–36.

Martini, E., Müller, C., 1971. Das marine Alttertiär in Deutschland und seine Einordnung in die Standard Nannoplankton Zonen. Erdöl und Kohle 24, 381–384.

McArthur, J.M., Howarth, R.J., Bailey, T.R., 2001. Strontium isotope stratigraphy: LOWESS version 3: best fit to the marine Sr-isotope curve for 0–509 Ma and accompanying look-up table for deriving numerical age. J. Geol. 109:155–170. http://dx.doi.org/10.1086/319243.

McConnaughey, T.A., 2003. Sub-equilibrium oxygen-18 and carbon-13 levels in biological carbonates: carbonate and kinetic models. Coral Reefs 22:316–327. http://dx.doi.org/10.1007/s00338-003-0325-2.

McConnaughey, T.A., Burdett, J., Whelan, J.F., Paull, C.K., 1997. Carbon isotopes in biological carbonates: respiration and photosynthesis. Geochim. Cosmochim. Acta 61: 611–662. http://dx.doi.org/10.1016/S0016-7037(96)00361-4.

Mertz-Kraus, R., Brachert, T.C., Reuter, M., Galer, S.J.G., Fassoulas, C., Iliopoulos, G., 2009. Late Miocene sea surface salinity variability and paleoclimate conditions in the Eastern Mediterranean inferred from coral aragonite $\delta^{18}O$. Chem. Geol. 262:202–216. http://dx.doi.org/10.1016/j.chemgeo.2009.01.010.

Miller, K.G., Wright, J.D., Fairbanks, R.G., 1991. Unlocking the ice house: Oligocene-Miocene oxygen isotopes, eustacy, and margin erosion. J. Geophys. Res. 96:6829–6848. http://dx.doi.org/10.1029/90JB02015.

Mingram, J., 1998. Laminated Eocene maar-lake sediments from Eckfeld (Eifel region, Germany) and their short-term periodicities. Palaeogeogr. Palaeoclimatol. Palaeoecol. 140:289–305. http://dx.doi.org/10.1016/S0031-0182(98)00021-2.

Mosbrugger, V., Utescher, T., Dilcher, D.L., 2005. Cenozoic continental climatic evolution of Central Europe. Proc. Natl. Acad. Sci. U. S. A. 102:14964–14969. http://dx.doi.org/10.1073/pnas.0505267102.

Muñoz, A., Ojeda, J., Sánchez-Valverde, B., 2002. Sunspot-like and ENSO/NAO-like periodicities in lacustrine laminated sediments of the Pliocene Villarroya Basin (La Rioja, Spain). J. Paleolimnol. 27:453–463. http://dx.doi.org/10.1023/A:1020319923164.

Ortega, P., Lehner, F., Swingedouw, D., Masson-Delmotte, V., Raible, C.C., Casado, M., Yiou, P., 2015. A model-tested North Atlantic Oscillation reconstruction for the past millennium. Nature 523:71–74. http://dx.doi.org/10.1038/nature14518.

Ottersen, G., Planque, B., Belgrano, A., Post, E., Reid, P., Stenseth, N.C., 2001. Ecological effects of the North Atlantic Oscillation. Oecologia 128:1–14. http://dx.doi.org/10.1007/s004420100655.

Pfeiffer, M., Lohmann, G., 2016. Greenland ice sheet influence on last interglacial climate: global sensitivity studies performed with an atmosphere–ocean general circulation model. Clim. Past 12:1313–1338. http://dx.doi.org/10.5194/cp-12-1313-2016.

Poulain, C., Lorrain, A., Mas, R., Gillikin, D.P., Dehairs, F., Robert, R., Paulet, Y.M., 2010. Experimental shift of diet and DIC stable carbon isotopes: influence on shell $\delta^{13}C$ values in the Manila clam *Ruditapes philippinarum*. Chem. Geol. 272:75–82. http://dx.doi.org/10.1016/j.chemgeo.2010.02.006.

Pross, J., 2001. Biostratigraphie organisch-wandiger Dinoflagellatenzysten in der Rupel-Abfolge (Unter-Oligozän) des Mainzer Becken. Mainz. Geowiss. Mitt. 30, 67–80.

Pross, J., Schmiedl, G., 2002. Early Oligocene dinoflagellate cysts from the Upper Rhine Graben (SW Germany): paleoenvironmental and paleoclimatic implications. Mar. Micropaleontol. 45:1–24. http://dx.doi.org/10.1016/S0377-8398(01)00046-9.
Prothero, D.R., 1994. The Late Eocene-Oligocene extinctions. Annu. Rev. Earth Planet. Sci. 22:145–165. http://dx.doi.org/10.1017/CBO9781107415324.004.
Prothero, D.R., Ivany, L.C., Nesbitt, E.A., 2003. From Greenhouse to Icehouse; the Marine Eocene-Oligocene Transition. Columbia University Press, NY, USA (541 pp).
Rasmusson, E.M., Wang, X., Ropelewski, C.F., 1990. The biennial component of ENSO variability. J. Mar. Syst. 1:71–96. http://dx.doi.org/10.1016/0924-7963(90)90153-2.
Reynolds, D.J., Richardson, C.A., Scourse, J.D., Butler, P.G., Hollyman, P., Román-González, A., Hall, I.R., 2017. Reconstructing North Atlantic marine climate variability using an absolutely-dated sclerochronological network. Palaeogeogr. Palaeoclimatol. Palaeoecol 465:333–346. http://dx.doi.org/10.1016/j.palaeo.2016.08.006.
Ritzkowski, S., Grimm, M.C., Hottenrott, M., 2011. Niederhessische Tertiärsenke. In: Deutsche Stratigraphische Kommission (Ed.), Stratigraphie von Deutschland IX. Tertiär, Teil 1. SDGG. 75, pp. 303–375.
Roeckner, E., Brokopf, R., Esch, M., Giorgetta, M., Hagemann, S., Kornblueh, L., Manzini, E., Schlese, U., Schulzweida, U., 2006. Sensitivity of simulated climate to horizontal and vertical resolution in the ECHAM5 atmosphere model. J. Clim. 19:3771–3791. http://dx.doi.org/10.1007/s00382-012-1612-9.
Román-González, A., Scourse, J.D., Butler, P.G., Reynolds, D.J., Richardson, C.A., Peck, L.S., Brey, T., Hall, I.R., 2017. Analysis of ontogenetic growth trends in two marine Antarctic bivalves *Yoldia eightsi* and *Laternula elliptica*: implications for sclerochronology. Palaeogeogr. Palaeoclimatol. Palaeoecol. 465:300–306. http://dx.doi.org/10.1016/j.palaeo.2016.05.004.
Roth, P.H., 1970. Oligocene calcareous nannoplankton biostratigraphy. Eclogae Geol. Helv. 63, 799–881.
Royer, C., Thébault, J., Chauvaud, L., Olivier, F., 2013. Structural analysis and paleoenvironmental potential of dog cockle shells (*Glycymeris glycymeris*) in Brittany, northwest France. Palaeogeogr. Palaeoclimatol. Palaeoecol. 373:123–132. http://dx.doi.org/10.1016/j.palaeo.2012.01.033.
Salzmann, U., Dolan, A.M., Haywood, A.M., Chan, W.-L., Hill, D.J., Abe-Ouchi, A., Otto-Bliesner, B., Bragg, F., Chandler, M.A., Contoux, C., Jost, A., Kamae, Y., Lohmann, G., Lunt, D.J., Pickering, S.J., Pound, M.J., Ramstein, G., Rosenbloom, N.A., Sohl, L., Stepanek, C., Ueda, H., Zhang, Z., 2013. Challenges in quantifying Pliocene terrestrial warming revealed by data-model discord. Nat. Clim. Chang. 3:969–974. http://dx.doi.org/10.1038/nclimate2008.
Scholz, D., Frisia, S., Borsato, A., Spötl, C., Fohlmeister, J., Mudelsee, M., Miorandi, R., Mangini, A., 2012. Holocene climate variability in north-eastern Italy: potential influence of the NAO and solar activity recorded by speleothem data. Clim. Past 8: 1367–1383. http://dx.doi.org/10.5194/cp-8-1367-2012.
Schöne, B.R., 2003. A "clam-ring" master-chronology constructed from a short-lived bivalve mollusc from the northern Gulf of California, USA. The Holocene 13:39–49. http://dx.doi.org/10.1191/0959683603hl593rp.
Schöne, B.R., 2008. The curse of physiology - challenges and opportunities in the interpretation of geochemical data from mollusk shells. Geo-Mar. Lett. 28:269–285. http://dx.doi.org/10.1007/s00367-008-0114-6.
Schöne, B.R., 2013. *Arctica islandica* (Bivalvia): a unique paleoenvironmental archive of the northern North Atlantic Ocean. Glob. Planet. Chang. 111:199–225. http://dx.doi.org/10.1016/j.gloplacha.2013.09.013.
Schöne, B.R., Oschmann, W., Houk, S.D., 2003. North Atlantic Oscillation dynamics recorded in shells of a long-lived bivalve mollusk. Geology 31:1037–1040. http://dx.doi.org/10.1130/G20013.1.
Schöne, B.R., Dunca, E., Fiebig, J., Pfeiffer, M., 2005. Mutvei's solution: an ideal agent for resolving microgrowth structures of biogenic carbonates. Palaeogeogr. Palaeoclimatol. Palaeoecol. 228:149–166. http://dx.doi.org/10.1016/j.palaeo.2005.03.054.
Stehlin, H.G., 1909. Remarques sur les faunules de Mammifères des couches éocènes et Oligocènes du Bassin de Paris. Bull. Soc. Geol. Fr. 9, 488–520.
Stepanek, C., Lohmann, G., 2012. Modelling mid-Pliocene climate with COSMOS. Geosci. Model Dev. 5:1221–1243. http://dx.doi.org/10.5194/gmd-5-1221-2012.
Strom, A., Francis, R.C., Mantua, N.J., Miles, E.L., Peterson, D.L., 2004. North Pacific climate recorded in growth rings of geoduck clams: a new tool for paleoenvironmental reconstruction. Geophys. Res. Lett. 31:L06206. http://dx.doi.org/10.1029/2004GL019440.
Torrence, C., Compo, G.P., 1998. A practical guide to wavelet analysis. Bull. Am. Meteorol. Soc. 79:61–78. http://dx.doi.org/10.1175/1520-0477(1998)079<0061:APGTWA>2.0.CO;2.
Trouet, V., Esper, J., Graham, N.E., Baker, A., Scourse, J.D., Frank, D.C., 2009. Persistent positive North Atlantic oscillation mode dominated the Medieval Climate Anomaly. Science 324:78–80. http://dx.doi.org/10.1126/science.1166349 (New York, N.Y.).
Van Simaeys, S., Vandenberghe, N., 2006. Rupelian. Geol. Belg. 9, 95–101.
Vandenberghe, N., Van Simaeys, S., Steurbaut, E., Jagt, J.W.M., Felder, P.J., 2004. Stratigraphic architecture of the Upper Cretaceous and Cenozoic along the southern border of the North Sea Basin in Belgium. Neth. J. Geosci. 83, 155–171.
Varma, V., Prange, M., Merkel, U., Kleinen, T., Lohmann, G., Pfeiffer, M., Renssen, H., Wagner, A., Wagner, S., Schulz, M., 2012. Holocene evolution of the Southern Hemisphere westerly winds in transient simulations with global climate models. Clim. Past 8:391–402. http://dx.doi.org/10.5194/cp-8-391-2012.
von Storch, H., Zwiers, F.W., 2001. Statistical Analysis in Climate Research. Cambridge University Press, Cambridge, UK (384 pp.).
Walliser, E.O., Schöne, B.R., Tütken, T., Zirkel, J., Grimm, K.I., Pross, J., 2015. The bivalve *Glycymeris planicostalis* as a high-resolution paleoclimate archive for the Rupelian (Early Oligocene) of central Europe. Clim. Past 11:653–668. http://dx.doi.org/10.5194/cp-11-653-2015.
Walliser, E.O., Lohmann, G., Niezgodzki, I., Tütken, T., Schöne, B.R., 2016. Response of Central European SST to atmospheric pCO_2 forcing during the Oligocene - a combined proxy data and numerical climate model approach. Palaeogeogr. Palaeoclimatol. Palaeoecol. 459:552–569. http://dx.doi.org/10.1016/j.palaeo.2016.07.033.
Weber, M.E., Clark, P.U., Kuhn, G., Timmermann, A., Sprenk, D., Gladstone, R., Zhang, X., Lohmann, G., Menviel, L., Chikamoto, M.O., Friedrich, T., Ohlwein, C., 2014. Millennial-scale variability in Antarctic ice-sheet discharge during the last deglaciation. Nature 510:134–138. http://dx.doi.org/10.1038/nature13397.
Wei, W., Lohmann, G., Dima, M., 2012. Distinct modes of internal variability in the global meridional overturning circulation associated with the southern hemisphere westerly winds. J. Phys. Oceanogr. 42:785–801. http://dx.doi.org/10.1175/JPO-D-11-038.1.
Werner, M., Haese, B., Xu, X., Zhang, X., Butzin, M., Lohmann, G., 2016. Glacial–interglacial changes in H218O, HDO and deuterium excess - results from the fully coupled ECHAM5/MPI-OM Earth system model. Geosci. Model Dev. 9:647–670. http://dx.doi.org/10.5194/gmd-9-647-2016.
Witbaard, R., Jenness, M.I., Vanderborg, K., Ganssen, G., 1994. Verification of annual growth increments in *Arctica islandica* L. from the North Sea by means of oxygen and carbon isotopes. Neth. J. Sea Res. 33, 91–101.
Witbaard, R., Duineveld, G.C.A., De Wilde, P.a.W.J., 1997. A long-term growth record derived from *Arctica islandica* (Mollusca, Bivalvia) from the Fladen Ground (Northern North Sea). J. Mar. Biol. Assoc. U. K. 77:801. http://dx.doi.org/10.1017/S0025315400036201.
Zachos, J.C., Dickens, G.R., Zeebe, R.E., 2008. An early Cenozoic perspective on greenhouse warming and carbon-cycle dynamics. Nature 451:279–283. http://dx.doi.org/10.1038/nature06588.
Zhang, X., Lohmann, G., Knorr, G., Purcell, C., 2014. Abrupt glacial climate shifts controlled by ice sheet changes. Nature 512:290–294. http://dx.doi.org/10.1038/nature13592.